

Refining an Inverse Dispersion method to Quantify Gas Sources on Rolling Terrain

by

NAN HU

A thesis submitted in partial fulfillment of the requirements for the degree of

Master of Science

Department of Earth and Atmospheric Sciences

University of Alberta

©Nan Hu, 2016

Abstract

In this thesis, an indirect methodology for estimating gas emission rate to the atmosphere from small surface point or area sources is investigated. More specifically, the thesis is a study of an “inverse dispersion” method which has become widely used for estimating ground-air gas fluxes (Q) from agricultural sources. Like all inverse dispersion methods, the “bLS” (for “backward Lagrangian stochastic”) method hinges on the placement of concentration detectors upwind and downwind from the source, allowing to determine the rise ($\Delta\bar{c}$) in mean gas concentration for which it is responsible. Also in common with the norm for “inverse dispersion”, a mathematical model of atmospheric dispersion is invoked so that the wanted source strength Q can be inferred from the measured concentration rise $\Delta\bar{c}$, which however must be supplemented with relevant meteorological information (such as mean wind direction and speed, and thermal stratification). In the case of “bLS,” the dispersion model is a backward Lagrangian stochastic model, which computes fluid element trajectories *backwards in time and space* from their arrival at the concentration detectors to their earlier point or points of contact with the source or sources.

An assumption inherent to most implementations of inverse dispersion method is that wind statistics in the atmospheric surface layer are horizontally-homogeneous (i.e. wind statistics vary only with height). It is of interest to establish how robust the inverse dispersion approach may be, when applied to quantify sources on land surfaces that are patently *not* flat and uniform – complications that result in horizontal variability of the wind statistics. In that context, this thesis analyses a trace gas dispersion experiment with multiple fixed point sources arrayed on gently rolling terrain, to investigate the performance of inverse dispersion using a well-

known bLS dispersion model (*WindTrax*) that, strictly speaking, is appropriate only for the case of horizontally-homogeneous winds. Despite the fact that measured mean wind speeds revealed spatial variation of order $\pm 10\%$ over the site, results of the inversion to estimate source strength indicate that the unwanted impact of this moderate terrain can be compensated by assigning every concentration detector its true height above local ground (for line-averaging optical detectors, this means the straightline light path transforms to a curved line). This strategy permits easy extension of a well proven method to conditions that, à priori, had been considered unsuitable; and the thesis culminates with application of the bLS approach to deduce an aggregate methane emission rate from a herd of (twenty) cattle confined within a long, narrow field of pasture.

Acknowledgements

This research has been funded by a grant from the Agricultural Greenhouse Gases Program (AGGP) of Agriculture and Agrifood Canada, and by the Natural Sciences and Engineering Research Council of Canada.

I wish to express my sincere gratitude to Dr. John D. Wilson for his encouragement, patient understanding, and guidance. I am also very grateful to Dr. Thomas K. Flesch, not only because the experiments he lead in the context of the AGGP research provided the research topic for my thesis, but also for his frequent and constructive guidance throughout this study. Dr. Xianmin Hu kindly assisted me with Latex issues, and generally helped me to adapt to circumstances at this university. Finally, thanks are also due to Dr. Gerhard Reuter and Dr. David Zhu, for serving on my examining committee.

Contents

Chapter 1. Introduction, Context and Methodology	1
1.1 Greenhouse gas research	1
1.2 Quantifying agricultural ground-to-air GHG fluxes	3
1.3 Lagrangian stochastic dispersion model	7
1.4 Statement of Monin-Obukhov Similarity Theory	9
1.5 Implementing an LS model to perform Inverse Dispersion	10
Chapter 2. Submitted Journal Article	12
1.6 Introduction	13
1.7 Inverse Dispersion Model	17
1.8 Lagrangian stochastic trajectory model (WindTrax)	18
1.9 Site and equipment	19
1.10 Inhomogeneity of the mean wind field	21
1.11 Terrain-following coordinate	21
1.12 Results	22
1.13 Conclusion	28
Chapter 3. Application: methane emissions from narrowly-penned cattle	36
3.1 Site, instruments and methodology	36
3.2 Inverse dispersion analysis and results	39
3.3 Conclusion	41

List of Tables

1.1	Performance of inverse dispersion	30
-----	---	----

List of Figures

2.1	A view of “plot 22” looking towards the north from the southern boundary fence.	31
2.2	Sketch of plot 22.	32
2.3	A view of the terrain, with cup anemometers positions and wind roses.	33
2.4	Different detector light paths	34
2.5	Mean performance $\langle Q_{\text{IDM}}/Q \rangle$ of the inverse dispersion method	35
3.1	A bird’s eye view of “plot 4,” looking north.	42
3.2	A ground-level view of “plot 4,” looking north.	43
3.3	A view of laser detector and path-deflecting plane mirrors.	44
3.4	Sketch of strips 1-5 in plot 4.	45
3.5	Daily cycle in inferred methane emission rate.	46

List of Acronyms

AGGP Agricultural Greenhouse Gases Program

ABL atmospheric boundary layer

ASL atmospheric surface layer

bLS backward Lagrangian stochastic

EF emission factor

GE gross energy intake

GHG Greenhouse Gas

IDM inverse dispersion method

IPCC Intergovernmental Panel on Climate Change

LS Lagrangian stochastic

MO Monin-Obukhov

MOST Monin-Obukhov similarity theory

MO-bLS Backward Lagrangian stochastic, MO velocity statistics

MO-fLS Forward Lagrangian stochastic, MO velocity statistics

MO-LS Lagrangian stochastic model, MO velocity statistics

SSE South-southeast

ZINST a specific measurement height

List of Symbols

- a_i conditional mean acceleration (function of position, velocity)
- b_{ij} coefficient of random forcing in generalized Langevin equation
- c instantaneous gas concentration
- C_0 dimensionless coefficient in Kolmogorov's model for the Lagrangian structure function
- $\Delta\bar{c}$ mean concentration rise
- $\partial\bar{c}/\partial z$ mean vertical concentration gradient
- h height of topography
- h' height of laser beam above local ground level
- $K_c(z)$ profile of eddy diffusivity of passive tracer gas
- k turbulent kinetic energy, $k = (\sigma_u^2 + \sigma_v^2 + \sigma_w^2)/2$
- $k_v (= 0.4)$ von Karman constant
- L Obukhov length
- n theoretical value for a dimensionless ratio
- Q ground-air gas flux
- Q_0 strength of a steady ground-level area source
- Q_{IDM} emission rate estimated by inverse dispersion method
- q instantaneous flux
- $\langle Q_{IDM}/Q \rangle$ mean value of the ratio Q_{IDM}/Q of inferred to true source strength
- Δt time step for computing particle trajectory
- $thres$ threshold value
- T temperature
- $T_* \equiv -\overline{w'T'}/u_*$ temperature scaling parameter

u_* friction velocity

\bar{u}_i components of the mean Eulerian velocity

$\overline{u_i c}$ components of the mean convective flux of c

$\overline{u'v'}$, $\overline{u'w'}$ velocity fluctuation covariances

ΔU_i increments in particle velocity over interval Δt

ΔX_i increments in particle position over interval Δt

x east-west coordinate

y north-south coordinate

z vertical coordinate

z_0 surface roughness length

Y_m proportion of gross energy in feed that is converted to methane (dimensionless)

$\bar{\beta}$ mean wind direction

δ ABL depth

δ_{ij} Kronecker delta ($= 1$ if $i = j$, $= 0$ if $i \neq j$)

σ standard deviation

$\sigma_{Q|Q}$ standard deviation of the ratio Q_{IDM}/Q of inferred to true source strength

$\sigma_u, \sigma_v, \sigma_w$ standard deviations of the Eulerian velocity fluctuations

$\phi_m()$ empirical dimensionless Monin-Obukhov function of ratio z/L

γ dry adiabatic lapse rate

ε turbulent kinetic energy dissipation rate

$d\xi_j$ Gaussian random number driving random velocity increment in direction j

Chapter 1. Introduction, Context and Methodology

The purpose of this chapter (Chapter 1) is to provide context and background for the main substance of my thesis. A number of disciplines have a need to measure or estimate surface-to-atmosphere exchange, to which end a variety of measurement techniques can (with provisos) be used. Here the specific context is Greenhouse Gas (GHG) fluxes from small agricultural sources (point sources or area sources whose horizontal span is of the order of 10 – 100 m), and the measurement technique is *indirect* (in contrast, for instance, to the “eddy covariance” approach that is in widespread use to measure the carbon balance of representative ecosystems across the world). Chapter 2, which has been submitted for publication, investigates the extension of a widely-used “inverse dispersion” technique for estimating ground-air exchange to quantify sources on terrain that — contrary to an assumption underlying the method — is *not* ideally flat. Chapter 3 briefly illustrates the application of this technique to deduce methane emissions from cattle grazing freely in long narrow paddocks, while Chapter 4 is a summary of the thesis.

Given, then, the context of the research, it is appropriate here at the outset to give some background on the inverse dispersion method that is the subject of Chapters 2 and 3, setting it against more direct methods. And because this technique (like most others) is inherently *micrometeorological* in its basis, the micrometeorology of the atmospheric surface layer will be briefly explained. It is perhaps worthwhile to note that although many academic disciplines relate at least tangentially to the content and concerns of this thesis, its scope falls most centrally into the subjects of Agrometeorology and Micrometeorology.

1.1 Greenhouse gas research

It is hardly necessary to state that in many countries, and especially those that are highly developed, there has been and remains much interest – driven by the international politics of Global Change – in quantifying greenhouse gas (GHG) emissions from the various economic

sectors. Setting aside carbon dioxide and the complex manner in which its uptake and release are affected by agriculture, it may be said that the most important *agricultural* greenhouse gases are methane and nitrous oxide (U.S. Environmental Protection Agency 2012). In ruminant animal agriculture (principally cattle and sheep), methane resulting from anaerobic digestion of carbohydrates in the rumen (enteric cellulose digestion) is emitted directly by the animals, while methane released from urine and manure is also important. Collectively, these methane sources make an important contribution to the increasing GHG content of the global atmosphere. Moss et al. (2000) estimated that enteric CH₄ emissions account for 12% of global GHG loading of the atmosphere (including both natural and anthropogenic sources), a greater 19% of the anthropogenic GHG loading, and fully 36% of agricultural CH₄ emissions; more recently Lassey (2008) estimated methane from agricultural sources accounts for 12% to 17% of global natural plus anthropogenic methane emissions. Switching to the national level, between 8% and 10% of Canada’s GHG emissions stem from agriculture, and of that amount 27% comes from beef production (not including dairy). It is understandable, then, that scientists in Canada and elsewhere¹ are engaged in the estimation of GHG fluxes to the atmosphere from farm animals and farm effluents, under the various management practices that prevail.

It is common to speak of “bottom-up” and “top-down” methods for the estimation of GHG emissions, and the work of this thesis falls in the former category — for it concerns a method to deduce the emission rate at a specific time and location from a specific source. However before proceeding it may be of interest to give (as context) the “tier 2 protocol” of the 2006 Intergovernmental Panel on Climate Change (IPCC) for cattle methane emissions:

$$\text{EF} [\text{kg}_{\text{CH}_4} \text{ head}^{-1} \text{ yr}^{-1}] = \frac{\text{GE} \times Y_m \times 365}{55.65}, \quad (1)$$

where EF is the “emission factor” (kg of methane emitted per cattlebeast per year), GE is gross

¹In Australia, agriculture produced 15.2% of net national emissions in 2011, of which non-dairy cattle contributed 115.5 kg/head from enteric fermentation (Australian National Greenhouse Gas Inventory Report 2013); in China, non-dairy cattle are estimated to produce 102.8 kg head⁻¹ yr⁻¹ from enteric fermentation (Xiangdong Hu 2010).

energy intake ($\text{MJ head}^{-1} \text{dy}^{-1}$), Y_m (dimensionless) is the proportion of gross energy in feed that is converted to CH_4 , and the factor on the denominator is the specific chemical energy content of methane (55.65 MJ kg^{-1}). Grown cattle consume of the order of 10 kg dry matter per day (5% of body weight, or more), and most feeds contain 8 to 12 MJ kg^{-1} . The factor Y_m (often given as a percentage rather than proportion) depends on diet, and ranges from about 0.03 (e.g. a feedlot diet of refined carbohydrates) to 0.1 (poor quality pasture). The lack of specificity in Eq. (25) is striking, and represents both its appeal and utility (in the context of gross national emissions estimates), and its weakness. Environment Canada (2013) — probably using Eq. (25) — estimates that non-dairy cattle in Canada contribute about $60 \text{ kg head}^{-1} \text{yr}^{-1}$ of methane from enteric fermentation. The need for confirmatory measurements that reflect the specifics of animal breeding and management practises is obvious.

1.2 Quantifying agricultural ground-to-air GHG fluxes

Denmead (1995) and McGinn et al. (2009) outline methods that can be used to quantify enteric methane emissions, and the present work falls squarely within the context of those papers. Let us temporarily take the perspective that ground level sources, in aggregate, can be represented as a steady ground-level area source (of strength “ Q_0 ” whose units, accordingly, are $\text{kg m}^{-2} \text{s}^{-1}$). This is especially germane for some types of agricultural GHG sources, e.g. nitrous oxide (N_2O) released from soil, and also represents a possible approach for the treatment of animal emissions from a herd or flock. Visualizing, then, an area source, the most tempting, immediate and rudimentary estimation of its strength Q_0 would be obtained by simply placing a chamber of some sort over a known surface area, and measuring the rate of accumulation of the gas in question. This, in crude terms, is the “chamber method,” which despite its known limitations is in widespread use.

Several types of chambers exist, e.g. those which measure the transient concentration and those which sustain a controlled and steady concentration within the chamber (flow-through type). In either case, it is highly probable that the emitting surface does not experience natural

conditions: unless great trouble is taken to do so, it will not be possible to mimic, inside the chamber, the naturally occurring temperature and humidity. And it is entirely impossible to mimic within the chamber a gusting wind with the natural surface layer wind statistics (regarding which, more below). If the rate-limiting step for the flux of interest is spatially isolated from the ground-air interface (e.g. a production reaction some distance into the soil) then it may be that these limitations of the chamber approach can be accepted. However in many situations the chamber method lacks credibility.

Still focusing on a steady area source (whose strength may vary from one typical 20–60 min micrometeorological averaging interval to the next), two categorically different types of mass balance provide an avenue for quantification. Sufficiently far downwind from the leading edge of the source, there is a near ground layer across which the vertical flux of the gas equals the (wanted) surface value (the “constant flux layer²”). Since the transport mechanism is convection, the instantaneous vertical flux of the gas at an elevated point P is

$$q(z_P) = w c \tag{2}$$

where $w = w(x, y, z, t)$ is the instantaneous vertical velocity of the air carrying the gas, and $c = c(x, y, z, t)$ is the instantaneous gas concentration. Of course the instantaneous flux q [$\text{kg m}^{-2} \text{s}^{-1}$] undergoes rapid variations, and so one simply averages this product to obtain an estimate

$$Q(z_P) = \overline{w c} \tag{3}$$

of the mean vertical flux. With the proviso that the measurement regime (wind field and gas concentration field) truly is such as to have yielded a constant flux layer, we have

$$Q(z_P) = Q_0 . \tag{4}$$

This is the “eddy covariance method,” a staple of micrometeorology and many related fields (agronomy, hydrology, biogeochemistry, and so forth). Of course there are nuances to the technique (e.g. Webb et al. 1980), but this, broadly, is its essence. Specialized fast response

²Many of the terms used in this thesis are central to the vocabulary of micrometeorology, and for scientists in that field require no explanation.

instruments, developed since roughly the 1950s, have enabled then commercialized this technique, which is regarded – hazardously (see Finnigan 1999; Finnigan et al. 2003; Finnigan 2008) – as the gold standard for measurement of ground-air exchange. In earlier years, prior to the development of fast response instruments, it was common in lieu of measuring the eddy flux directly to employ a “flux gradient method,” central to which is the adoption of an eddy diffusion relationship

$$Q(z) = -K_c \frac{\partial \bar{c}}{\partial z} \quad (5)$$

where $K_c(z)$ is the eddy diffusivity and $\partial \bar{c} / \partial z$ is the mean vertical concentration gradient. There are many variants of flux gradient technique, and just as for eddy covariance there are limitations to its applicability (Wilson et al. 2001). In particular, one requires *a long fetch of source*, and small mean concentration differences along the vertical must be determined with adequate accuracy.

Two types of mass balance were mentioned above. In the circumstance that one *has* the luxury of a long fetch of source, one may invoke the assumption of a height-independent vertical flux (as outlined above) and mass conservation implies Eq. (4). Conversely, if one has a short fetch (upwind distance) of source, it is feasible to invoke the notion that “what goes up must blow downstream”, or, in effect, perform a mass balance on the walls of an imaginary control volume encompassing the source. In the simplest case that there is crosswind (y) symmetry of the source and that the concentration of the gas upwind of the source vanishes (“no background concentration”) then it is only necessary to sum up the horizontal gas flux across a vertical coordinate plane standing downwind ($x = X$) of all sources, viz.

$$Q_0 = \int_{z=0}^{\infty} \bar{u} \bar{c} dz \quad (6)$$

where $\bar{u} \bar{c}$ is the average of the alongwind convective flux of the gas, varying with height z across the plume of gas emanating from the source (note: u designates the horizontal velocity component in a coordinate system aligned with the mean wind³). To a good approximation (i.e.

³Mean wind direction is usually found to be practically invariant across the atmospheric surface layer; an

within $\sim 10 - 20\%$) this may be simplified by neglecting the part of the horizontal flux that is carried by velocity fluctuations, viz.

$$Q_0 = \int_{z=0}^{\infty} \bar{u} \bar{c} dz = \int_{z=0}^{\infty} [\bar{u} \bar{c} + \overline{u'c'}] dz \approx \int_{z=0}^{\infty} \bar{u} \bar{c} dz \quad (7)$$

(the Reynolds decomposition $u = \bar{u} + u'$ has been invoked to expand the uc product). When based on the approximation inherent to eq. (7), the “Integrated Horizontal Flux” technique requires only slow response instruments (e.g. cup anemometers may be used to measure the vertical profile $\bar{u}(z)$ of the mean wind). A further attraction of the method is that *it makes no assumption as to the field of the wind statistics*, i.e. it is valid even if the measurement site features a disturbed wind field. However the vertical integration does require multi-level instrumentation, and this is the attraction of methods that *combine* the mass balance principle with a model of spatial field of mean concentration caused by the source. And so soon as one’s measurement procedure blends observations with a model, one is on the territory of a “data assimilation” approach. In this thesis, the term “inverse dispersion” will be used.

An early form of the latter is represented by the “Theoretical Profile Shape” method of Wilson et al. (1982). Here the source was specifically circular (radius R), and a single measurement of the $\bar{u} \bar{c}$ product was to be made at the centre of the plot at a specific height ZINST. The latter had to be chosen according to the value of the radius R . Based on the calculated concentration field produced by the source, a nomogram permitted the deduction of source strength Q_0 from measured $\bar{u} \bar{c}$. Flesch et al. (1995) generalized this method for arbitrary shapes of source, introducing what became known as the “backward Lagrangian stochastic” (bLS) method for inverse dispersion on the micrometeorological scale.

The balance of this chapter provides some background on the Lagrangian stochastic model⁴, and on the near-ground wind field that controls the computed trajectories linking a source to a concentration detector.

exception is the case where the latter encompasses a deep roughness sublayer, such as a tall plant/forest canopy.

⁴The Lagrangian stochastic model is sometimes referred to as a (turbulent) ‘trajectory simulation model’.

1.3 Lagrangian stochastic dispersion model

A Lagrangian stochastic model (Thomson 1987; Wilson and Sawford 1996; Thomson and Wilson 2013) mimics the trajectories of thousands of tracer “particles,” each trajectory being the summation of discrete changes in particle position ΔX_i and velocity ΔU_i over a time step Δt that are computed as

$$\Delta U_i = a_i \Delta t + b_{ij} d\xi_j, \quad (8)$$

$$\Delta X_i = (U_i + \bar{u}_i) \Delta t. \quad (9)$$

Here \bar{u}_i are the components of the mean Eulerian velocity, while the U_i are the components of the Lagrangian velocity *deviation* from the \bar{u}_i . The coefficients a_i and b_{ij} of the “generalized Langevin equation” are functions of position and velocity, and $d\xi_j$ is a Gaussian random number (drawn independently for each time step from a population having zero average and variance Δt). Eq. (8) is sometimes referred to as a ‘generalized Langevin equation,’ and indeed for the simplest regime of turbulence (viz. stationary, homogeneous and isotropic turbulence) the model does reduce to three independent Langevin equations, governing motion on the three axes.

We would like a specification of the model coefficients that is appropriate to trajectories within the atmospheric surface layer, and we will assume velocity statistics within that layer are horizontally homogeneous (Section 1.4 below defines the statistics of the wind field in the atmospheric surface layer). For simplicity we now restrict the discussion to two directions of motion (alongwind x and vertical z). The coefficients (a_u, a_w) are the components of the conditional mean particle acceleration (specified below), while the coefficients b_{ij} of the random forcing terms reduce to

$$b_{ij} = \delta_{ij} \sqrt{C_0 \varepsilon}, \quad (10)$$

where $\varepsilon = \varepsilon(z)$ is the turbulent kinetic energy dissipation rate and C_0 is a dimensionless coefficient originally introduced by Kolmogorov. With the approximations, (i) that the joint probability density function g_a for the Eulerian velocity fluctuations (u', w') is Gaussian, and

(ii) that the velocity correlation is height invariant ($-\overline{u'w'} \equiv u_*^2$, where u_* is the friction velocity) throughout the atmospheric surface layer, and (iii) that the standard deviation of the alongwind velocity fluctuation $\sigma_u = \text{constant} = \alpha u_*$ with $\alpha \approx 2$ (whereas $\sigma_w = \sigma_w(z)$), one obtains the following prescription for the remaining coefficients:

$$a_u = -\frac{b^2}{2\sigma^2} [U \sigma_w^2 + W u_*^2], \quad (11)$$

$$a_w = -\frac{b^2}{2\sigma^2} [W \sigma_u^2 + U u_*^2] + \frac{1}{2} \frac{\partial \sigma_w^2}{\partial z} \left[1 + \frac{\sigma_u^2 W^2 + u_*^2 U W}{\sigma^2} \right], \quad (12)$$

where

$$\sigma^2 = \sigma_u^2 \sigma_w^2 - u_*^4, \quad (13)$$

$$b = \sqrt{C_0 \varepsilon}. \quad (14)$$

The two-dimensional Lagrangian stochastic (LS) model defined by Eqs. (8-14) is a special case of Thomson's (1987) more general model for vertically-inhomogeneous Gaussian turbulence. Particles are released from the source with a velocity chosen randomly from g_a , i.e. with the correct correlation between (U, W) . At every step along the trajectory the Eulerian velocity statistics $(\sigma_w, \varepsilon, \bar{u})$ appearing in the algorithm are re-evaluated at the particle's present height Z , and the time step Δt is evaluated as

$$\Delta t = \frac{2\sigma_w^2}{C_0 \varepsilon}, \quad \mu \ll 1 \quad (15)$$

where $2\sigma_w^2/(C_0 \varepsilon)$ is an effective Lagrangian velocity decorrelation timescale. Of course, one can implement the model only if one has somehow managed to prescribed these various Eulerian properties of the wind field (i.e. $\sigma_u, \sigma_w, \varepsilon, \bar{u}$), and to that end we invoke and exploit a *theory* for the atmospheric surface layer (Monin-Obukhov similarity theory, MOST) that furnishes these needed inputs so soon as one has provided the measured values of a manageable few "external" governing parameters; among the latter, the friction velocity u_* is salient.

1.4 Statement of Monin-Obukhov Similarity Theory

Monin-Obukhov similarity theory (MOST) is the working model of the horizontally homogeneous atmospheric surface layer (“hh_ASL”). Briefly stated, Monin and Obukhov (a) observed that over flat, even, uniform terrain there exists a shallow ground-based layer across which the mean (kinematic) vertical fluxes of heat and momentum ($\overline{w'T'}$, $\overline{u'w'}$, $\overline{v'w'}$, where T' is the temperature fluctuation) can be treated as effectively height independent (“constant stress layer” or “constant flux layer”); and, (b) proposed (most fruitfully) that the signs and magnitudes of those fluxes, along with height z above ground and the coefficient of thermal expansion g/T_0 , control the statistics of velocity and temperature. Other fluxes, e.g. humidity, would add to this and complete the picture, fixing humidity (and joint wind-humidity) statistics; and it was explicit that this idealized structure would obtain only within a layer $z_0 \ll z \ll \delta$, where z_0 is the surface roughness length and δ the depth of the atmospheric boundary layer (ABL). Thus, MOST does not apply within the so-called “roughness sublayer” where additional length scales (characterizing the surface and/or a vegetation canopy) complicate the picture. It was subsequently found useful to add δ to the set of controlling scales.

The friction velocity is defined most fundamentally in terms of the kinematic momentum fluxes as

$$u_*^4 = (\overline{u'w'})^2 + (\overline{v'w'})^2, \quad (16)$$

such that $\tau = \rho u_*^2$ (where ρ is the air density) is the magnitude of the shear stress on ground. A dimensional analysis following the tenets of MOST gives what are now well proven relationships for quantities such as the mean wind shear

$$\frac{kz}{u_*} \frac{\partial \bar{u}}{\partial z} = \phi_m \left(\frac{z}{L} \right) \quad (17)$$

where $k_v (= 0.4)$ is the von Karman constant, and ϕ_m is a dimensionless empirical function of the ratio z/L of height to the Obukhov length L , which is defined

$$L = \frac{-u_*^3 T_0}{k_v g \overline{w'T'}}. \quad (18)$$

Similarly the vertical gradient in mean temperature is given by

$$\frac{kz}{T_*} \left(\frac{\partial \bar{T}}{\partial z} - \gamma \right) = \phi_h \left(\frac{z}{L} \right) \quad (19)$$

where $T_* \equiv -\overline{w'T'}/u_*$ is the “temperature scaling parameter” and γ is the dry adiabatic lapse rate.

Suffice to say that the empirical functions of MOST (i.e. ϕ_m, ϕ_h and so on) have been the object of investigation in numerous classic experiments, and can be considered known. Integration of Eq. (17) gives a formula for the mean horizontal wind velocity at all heights in the ASL, provided one can supply the values of u_*, L (or equivalently u_*, T_*), which is easily done by operating a sonic anemometer. Provided the experimental situation is not such as to render the assumptions underpinning MOST invalid, these laws imply that a single instrument can provide *complete* information on velocity statistics (and indeed joint velocity-temperature statistics) across the ASL. We shall assume the surface cover to be shallow, such that the existence of a roughness sublayer can be ignored, and the MOST profiles, extrapolated down to the roughness height z_0 , describe the entire layer to a satisfactory level of approximation.

1.5 Implementing an LS model to perform Inverse Dispersion

Briefly, to use the inverse dispersion method along the lines explored in this thesis it is necessary to measure the mean concentration of the target gas both upwind (“ \bar{c}_u ”) and downwind (“ \bar{c}_d ”) from the source, and additionally one must measure four necessary meteorological parameters: the mean wind direction $\bar{\beta}$, the mean wind speed \bar{u} at one height (“reference speed,” say U), the Obuhov length L and aerodynamic roughness length z_0 , and to invoke an atmospheric dispersion model to infer the emission rate Q necessary to “explain” the observed concentration rise ($\bar{c}_d - \bar{c}_u$). This model must provide a *theoretical* value for the dimensionless ratio

$$n = \frac{U (\bar{c}_d - \bar{c}_u)}{Q} \quad (20)$$

that takes into account the meteorological conditions and the known information — which may be complete or partial — regarding the particulars of the source and its placement relative to

the detectors. The estimated flux Q_{IDM} is determined from the measured information (“meas”) as

$$Q_{\text{IDM}} = \frac{[U (\bar{c}_d - \bar{c}_u)]^{\text{meas}}}{n} \quad (21)$$

and ideally $Q_{\text{IDM}}/Q = 1$ (where Q is the true emission rate, in general unknown).

The following chapter (Chapter 2) is the main substance of this M.Sc. thesis, a paper that has been submitted (September 19th, 2015) to *Agricultural and Forest Meteorology*. It addresses the adaptation of the inverse dispersion approach outlined above to the (common) circumstance that the wind field at the site in question *deviates* (albeit perhaps only mildly) *from being horizontally homogeneous* — as is obviously the case so soon as the terrain is not perfectly flat. The question of how best to implement inverse dispersion on mildly rolling terrain is explored with reference to a trace gas dispersion experiment performed for that specific purpose. Chapter 3, as yet not submitted, sketches the application of the technique in an experiment to determine cattle methane emissions, while Chapter 4 gives some closing remarks.

Chapter 2. Submitted Journal Article

This chapter is the manuscript of a journal article that has been submitted⁵ (29 September 2015) to *Agricultural and Forest Meteorology* (ISSN: 0168-1923). Tables and figures appear in their correct order at the end of this chapter.

Title

Refining an inverse dispersion method to quantify gas sources on rolling terrain

Journal

Submitted (29 September 2015) to *Agricultural and Forest Meteorology* (ISSN: 0168-1923)

Authorship

This manuscript has been co-authored by myself (Nan Hu), Dr. T.K. Flesch (Research Associate, Earth & Atmospheric Sciences, U. Alberta), Dr. J.D. Wilson (my supervisor, Earth & Atmospheric Sciences, U. Alberta), and Dr. V. Baron (Agriculture and Agrifood Canada). My own contribution to the paper was to carry out the analysis of experimental data collected by the other authors. I have also participated in subsequent experimental work to gain first hand knowledge of the experimental technique.

Abstract

It is common practice to estimate ground-air gas fluxes (Q) from agricultural sources by inverse dispersion, placing detectors upwind and downwind from the source to determine mean gas

⁵Subsequently to my thesis defense, reviews have been received. Some revisions have been requested, however this chapter has not been modified relative to the draft presented for examination prior to the defense on 4 December 2015.

concentration (\bar{c}). Often however, topography compromises an assumption that is (normally) inherent to the inverse dispersion methodology, namely that wind statistics in the atmospheric surface layer are “undisturbed” (i.e. horizontally-homogeneous). We analysed a trace gas dispersion experiment with multiple fixed point sources on gently rolling terrain, to investigate the performance of inverse dispersion using a dispersion model (WindTrax) that (strictly) is appropriate only for the case of horizontally-homogeneous flow. Despite the fact that measured mean wind speeds revealed spatial variation of order $\pm 10\%$ over the site, results of the inversion to estimate source strength indicate that the unwanted impact of this moderate terrain on the idealized $\bar{c} - Q$ relationship can be compensated by – in effect – postulating an undisturbed Monin-Obukhov flow in a terrain following height coordinate, such that (e.g.) light paths of the line-averaging concentration detectors are treated as curves having everywhere the true height above ground. This strategy permits easy extension of a well proven method to conditions that, à priori, had been considered unsuitable. We also used the measurements to study the influence (on the accuracy of retrieved Q) of discretionary elements of inverse dispersion procedure. These sensitivity studies addressed optimal placement of detectors relative to the source(s); data rejection criteria, such as threshold values for the friction velocity and the Obukhov length; exclusion of mean wind directions that confound the “upwind/downwind” concentration differences; and the impact of alternative spatial representations of the source, supposing one had but *partial* information in that regard.

Keywords: Agricultural gas emissions; Flux measurements; Greenhouse gas emissions; Inverse dispersion

1.6 Introduction

This paper is concerned with the practicability of measuring gas exchange between small surface sources and the atmosphere by inverse dispersion (Wilson et al. 2012), specifically under the circumstance that an assumption of uniformity (horizontal-homogeneity) of the wind field cannot

strictly be justified and/or the spatial distribution of the source or sources is only partially determined. Though this does not restrict the generality of our findings, the context of the paper is the task of measuring agricultural gas emissions, from an individual farm in its entirety, or from some component such as a single paddock or a group of confined animals or a waste lagoon; such types of measurements spurred the work, and the analysis of a trace gas dispersion experiment from point sources over gently rolling terrain will be central to what follows.

It is well known that direct flux measurements by eddy covariance or by the flux-gradient method are feasible only at sites satisfying certain practical limitations: for instance the flow itself needs to be (nominally, and in the statistical sense) horizontally uniform, in order that the needed assumption of a vanishingly small mean vertical velocity be justifiable; and the source needs to be sufficiently extensive as to generate a constant flux layer of the gas in question (equivalently, the flux footprint must not extend off the source). In addition eddy covariance requires the existence of a suitably rapid gas detector, while a flux-gradient method demands that small mean concentration differences along the vertical can be determined with adequate accuracy.

An inverse dispersion method (IDM) relaxes some of these requirements. Defined briefly, using IDM one measures the mean concentration of the target gas both upwind (“ \bar{c}_u ”) and downwind (“ \bar{c}_d ”) from the source, along with necessary meteorological information (normally the mean wind direction $\bar{\beta}$, the mean wind speed U at one height (“reference speed”), the Obuhov length L and aerodynamic roughness length z_0), and one invokes an atmospheric dispersion model to infer the emission rate Q necessary to “explain” the observed concentration rise ($\bar{c}_d - \bar{c}_u$). The model must provide a *theoretical* value for the dimensionless ratio

$$n = \frac{U(\bar{c}_d - \bar{c}_u)}{Q} \quad (22)$$

that takes into account the meteorological conditions and the known information — which may be complete or partial — regarding the particulars of the source and its placement relative to the detectors. The estimated flux Q_{IDM} is determined from the measured information (“meas”)

as

$$Q_{\text{IDM}} = \frac{[U(\bar{c}_d - \bar{c}_u)]^{\text{meas}}}{n} \quad (23)$$

and ideally $Q_{\text{IDM}}/Q = 1$ (where Q is the true emission rate, in general unknown).

An IDM method, as defined above, obviously is not assumption free: one requires a model, and it is incumbent on the analyst to ensure that IDM is executed (only) under such circumstances as legitimise the pretence that the model is a “true” model of the relationship between $(\bar{c}_d - \bar{c}_u)$ and the unknown flux Q , whose determination is the target of the exercise. We return to this (potential) flaw of IDM (i.e. imperfect modelling) below. But before doing so it is appropriate to stress that in suitable circumstances IDM is a convenient method with good accuracy. IDM is not restricted to small sources and does not necessarily require the measurement of a very small concentration difference (i.e. one may be able to arrange detectors such that $\bar{c}_d - \bar{c}_u$ is large enough to be measurable with whatever slow response detectors one has available); unlike some other possible techniques (such as flux chambers), though in common with eddy covariance, IDM is (or can be) a non-interfering method (sensors can be placed out of the way of farm operations); and as to accuracy, as a rough specification, when IDM is implemented according to established guidelines (Flesch et al. 2004) it is found that individual 30-min determinations of Q typically scatter around the truth with a standard deviation of about 20% or less, and a bias of no more than about 5%. In the past decade many groups have estimated agricultural gas emissions using free software **WindTrax**⁶, which facilitates IDM and encapsulates a Lagrangian stochastic (LS) trajectory model to compute the “magic number” n (Wilson et al. 2012).

Returning to the opening paragraph above, the theme of this paper is to address factors that may compromise the accuracy of IDM. As with any other flux measurement method one might invoke, an IDM measurement is liable to take place in a context that entails *imperfect or*

⁶“WindTrax” is a widely used free software package written by Brian Crenna that encodes forward and backward LS models into a graphical user interface (GUI) facilitating the application of the inverse dispersion method for small sources. It is applicable on the micrometeorological scale, and assumes the state of the surface layer is described by Monin-Obukhov similarity theory.

incomplete prior information, or even disinformation. For instance, it is common – indeed usual – to adopt a dispersion model (e.g. WindTrax) for IDM that is predicated on the wind field at the site being horizontally-homogeneous, and accurately described by the Monin-Obukhov theory of an ideal atmospheric surface layer. But is the wind field *truly* uniform? One may be very well aware that it is not (e.g. irregularity of the topography might be an obvious factor). What is the penalty if one ignores this? A second (and in practice, equally common) type of incomplete (and/or potentially erroneous) prior information arises from one’s prescription of the source: one might for instance know (or believe, or guess) that it consists of a set of N steady point sources all of equal strength, and having known locations (as was the case in the tracer experiment that will be described and analysed below). Alternatively one might have *partial* information (true or otherwise): e.g. that the emissions originate from a group of *moving* point sources, not necessarily of equal strength, and having uncontrolled and (perhaps) unknown locations within a prescribed (or guesstimated) perimeter.

Section 2 will sketch the basis for inverse dispersion on the micrometeorological scale. Section 3 will describe a trace gas dispersion experiment that was executed on rolling terrain, using continuous point sources of equal strength (in aggregate, “ Q ”) and known location (these nominally simulated a herd of cows), and with line-averaged concentrations measured upwind and downwind. The novelty of the paper lies in Section 4, an analysis of the experiment and (more specifically) of the *quality* of inverse dispersion estimates of Q in relation to various strategies one might hypothetically invoke to compensate for, or minimise the negative impact of: (a) incomplete information about the spatial structure of the source, and (b) deviation of the wind statistics from MOST due to topography. Possible strategies include data filtering to reject measurement intervals during extreme thermal stratification (a step which has been found advantageous even when IDM is applied on ideal terrain), adoption of a terrain-following height coordinate in defining the experimental geometry, and alternative strategies to represent the source (e.g. actual point sources aggregated as an area source). The impact of strategies is revealed by a series of sensitivity studies whereby the “quality” of IDM estimates is gauged by

statistics of the ratio Q_{IDM}/Q , including its mean value $\langle Q_{\text{IDM}}/Q \rangle$, whose difference from unity is the “bias,” and its standard deviation $\sigma_{Q|Q}$ about that mean.

In what follows, Eulerian properties such as the wind velocity components along coordinates (x, y, z) are represented in lower case, e.g. (u, v, w) . The Reynolds decomposition splits the local, instantaneous value of u into its mean and fluctuation as $u = \bar{u} + u'$, and we may define a mean “cup wind speed” as $\bar{s} = \sqrt{\overline{u^2 + v^2}}$. Lagrangian quantities will be represented in upper case (e.g. particle height Z and vertical velocity W), with temperature (T) being an exception. Because in the practice of IDM one will be tracking the orientation of the wind relative to (e.g.) the boundaries of a rectangular paddock treated as an area source, we shall define x as the east-west coordinate (increasing towards the east) and y as the north-south coordinate increasing to the north. Further variables will be defined where they are first encountered.

1.7 Inverse Dispersion Model

Establishing a theoretical relationship between the strength Q of a given source and the resulting mean concentration field \bar{c} is a familiar problem in micrometeorology, and it is usual to divide the overall problem into two parts: specification (in statistical terms) of the wind and turbulence field that will advect and mix the gas away from the source (the “flow problem”); and, *given* those statistics, solution of the “dispersion problem.” The latter could (for instance) entail solving an advection-diffusion equation

$$\bar{u}(z) \frac{\partial \bar{c}}{\partial x} + \bar{v}(z) \frac{\partial \bar{c}}{\partial y} = \frac{\partial}{\partial z} \left[K_c(z) \frac{\partial \bar{c}}{\partial z} \right] + \frac{\partial}{\partial y} \left[K_c(z) \frac{\partial \bar{c}}{\partial y} \right] \quad (24)$$

where $\bar{u}(z), \bar{v}(z)$ are the profiles of the horizontal velocity components and $K_c(z)$ is the profile of the eddy diffusivity of the gas, usually assumed to be a “passive tracer.” Eq. 24 is an approximate statement of mass conservation for a steady (sustained) source, and would be solved with appropriate boundary conditions; the fact of the profiles being indicated as functions of height z alone announces that (if Eq. 24 were the model adopted) the wind field and the eddy

diffusivity had been assumed horizontally homogeneous⁷.

Indeed despite the rolling topography at site of the experiments to be described, all inversions *were* performed by treating the flow *as if* it were horizontally homogeneous⁸, and characterized by the Monin-Obukhov similarity theory (MOST). Within the scope of that approximation, a single sonic anemometer provided all needed information on the flow, as characterized by the friction velocity u_* , the Obukhov length L , the mean wind direction $\bar{\beta}$ and the surface roughness length z_0 . Although the experimental site featured a thin canopy of grass, we assumed that MOST profiles, extrapolated down to the roughness height, describe the entire layer to a satisfactory level of approximation.

1.8 Lagrangian stochastic trajectory model (WindTrax)

As indicated above, a flux measurement by inverse dispersion can be based on any appropriate dispersion model. However following Flesch et al. (1995, 2004) a particularly flexible and convenient procedure is to exploit a *backward* Lagrangian stochastic (LS) trajectory model, which computes the $\bar{c} - Q$ relationship (the magic number n) by computing an ensemble of representative turbulent trajectories connecting the detector and the source: the adjective “backward” applies because these trajectories are computed backwards in time and space, i.e. one computes a set of trajectories that end, eventually, at the detector. For simplicity, and as here, it is usually assumed that wind statistics obey MOST, and specialized software (e.g. WindTrax) has evolved to facilitate inverse dispersion using “MO-bLS” (because in the case of point sources a *forward* model is needed, we may speak also of MO-fLS; or in all embracing terms, inverse dispersion by MO-LS). Numerous groups have applied MO-LS to deduce emissions from various sources,

⁷Several other assumptions are implicit in Eq. 24, most notably the representation of convective transport by the velocity fluctuations as a diffusion process. As this is not the model of primary interest here, it is not necessary to further elaborate the basis for this specific advection-diffusion model.

⁸In principal one could have adopted a three-dimensional wind field (e.g. Wilson et al. 2010), however the needed flow computation greatly complicates application of the inverse dispersion approach.

often in an agricultural or waste management context. Examples include emissions of ammonia from barns (Harper et al. [2010]), from fields (Sanz et al. [2010]), from waste storage ponds (Flesch et al. [2013]), from feeder cattle (Todd et al. [2011]), from beef cattle (Laubach et al. [2008]) and from grazing cattle (McGinn et al. [2011]).

WindTrax adopts the LS model given by Thomson (1987) for vertically-inhomogeneous Gaussian turbulence (i.e. the probability density function for velocity is assumed to be Gaussian), a common choice for the atmospheric surface layer. In terms of the needed Eulerian quantities, trajectories are “driven” by the mean Eulerian velocity components (\bar{u}, \bar{v}) ; the turbulent velocity variances $(\sigma_u^2, \sigma_v^2, \sigma_w^2)$; the velocity fluctuation covariances $(\overline{u'v'}, \overline{u'w'}, \overline{v'w'})$; and the turbulent kinetic energy dissipation rate (ε) . It is the role of the experimenter to provide these data, and (as noted earlier), with the assumption that MOST applies, measurements from a single sonic anemometer yield all needed information.

1.9 Site and equipment

In preparation for an inverse dispersion campaign to measure methane emissions from cattle, a tracer dispersion experiment was performed in “plot 22” at the Lacombe Research Centre (Agriculture and Agri-Food Canada, 52.457393 N, 113.765297 W). The topography and instrument layout at the site are indicated by Figures (2.1–2.3); contours on Figure 2.3 were derived from digital elevation files covering the township (TWP 40, ranges 27 and 26 west of the 4th meridian) that were purchased from AltaLIS (“LiDAR15 DEM”, post spacing 15 m, vertical resolution 0.3 m). The origin of the coordinate system for the analysis to follow coincides with the post in the SW corner of plot 22.

Eight point sources of tracer methane were distributed at known positions, within an overall area of about 20 m \times 120 m, in the gently rolling pasture (mean roughness length about 0.08 m). The distribution of the sources within a long, narrow area echoed the intended design for the eventual work with cattle, which was to ensure that for almost all mean wind directions $\bar{\beta}$ there should be significantly different upwind and downwind concentrations, despite the inevitable

short term fluctuations of wind direction about the mean. The point of the tracer experiment was to evaluate the accuracy with which the inverse dispersion method would return the (in this case, known) emission rate Q , without accounting for any disturbance to the surface layer flow over the site: that is, WindTrax would be applied as if the terrain were perfectly flat and uniform, with the trajectory model driven by single point velocity statistics supplied by a sonic anemometer (Campbell Scientific CSAT3), those statistics being height-extrapolated using Monin-Obukhov similarity theory. A set of matched cup anemometers measured the degree of spatial variation of the wind (see Section 1.10), but those data were not used in any way for the inversion of $(\bar{c}_u - \bar{c}_d)$ to obtain Q_{IDM} .

The tracer methane was released from a cylinder at a rate that was controlled by a flow regulator, and flowed along equal-lengthed lines to the release points at 0.8 m AGL. As a backup check, cylinders were weighed before and after being consumed. Release rate was controlled at 0.97 kg hr^{-1} (from 16th to 18th August) and 0.73 kg hr^{-1} (21th and 22th August). During suitable winds, gas was released continuously and measurements were aggregated to form 30 min averages. A total of 107 such intervals were available for analysis.

The needed concentration measurements were made using line-averaging laser gas detectors (Boreal Laser Gasfinder 2), one detector (“C39”) running north-south on the west side and another (“C15”) on the east side of the source distribution, with path lengths of 110 m. Fig.2.2 is a schematic of the layout, and it should be evident that the distribution of the sources along the long axis (y) of the plot would have negligible impact on the line-averaged concentrations sensed by the laser detectors (this being a key attribute of the experimental design). Because of the rolling topography $h = h(x, y)$, the height $z'(x, y) = z - h(x, y)$ of the laser beams above the ground varied along the light path and differed for the two lasers. To obtain an approximate representation of $z'(x, y)$ for each path we sighted a (vertical) measuring rod, using a telescope mounted on top of the laser (6.5 cm above the laser; this offset was corrected). From these measurements the *mean* path heights (relative to local ground level) for laser C39 (on the west) and laser C15 (on the east side of the source) were respectively $\langle z'_{\text{C39}} \rangle = 1.43 \text{ m}$ and $\langle z'_{\text{C15}} \rangle = 1.65$

m (i.e. the angle bracket signifies an average along the light path).

1.10 Inhomogeneity of the mean wind field

In order to procure some measure of the degree of inhomogeneity of the wind field at the site, mean wind speeds were measured by cup anemometers (Climet 011-4) at twelve locations (height $z = 1.12$ m) distributed around the trace gas sources at the locations indicated on Figure 2.3. Individual fifteen minute mean speeds were normalized relative to the value at one location (the reference location “**P**”, not far from the middle of the array of point sources), and these normalized mean speeds were binned (averaged) within sectors ($\bar{\beta} = \beta_0 \pm 22.5^\circ$) of mean wind direction centred on the 8 cardinal directions $\beta_0 = 0, 45, 90, \dots, 315^\circ$ (mean wind direction $\bar{\beta}$ at a single point in the array was assumed to characterize the overall orientation of the flow). Then for each wind direction sector a mean relative windspeed was defined by averaging over all (270) runs for which mean windspeed at **P** exceeded 2.5 m s^{-1} , this threshold being chosen to ensure any period during which cups may have stalled would not be included in the averaging.

Figure 2.3 indicates that, relative to the reference point **P**, relative mean wind speeds varied from as low as about 0.9 to as high as about 1.05, i.e. variations of mean wind speed from place to place over the terrain did not exceed about $\pm 10\%$. In terms of interpretation, at cup #9 (northernmost on the main transect) which sat in a gulley, the increased mean wind speed for a SSE wind can be understood as being a channeling effect. A quantitative comparison of the relative windspeed data with a linearized numerical flow model has been undertaken, and if one excludes wind directions for which steep terrain lay upwind of the anemometer array then there was a fair quantitative accord (not shown here). Thus in terms of the *degree* of inhomogeneity of the flow, it can be stated with certainty that deviations of order 10% occurred. Whether or not comparable changes occurred in higher order wind statistics (e.g. σ_w) is a matter of conjecture.

1.11 Terrain-following coordinate

The above noted spatial variation of the measured mean wind speeds (at fixed height above ground) disapproved any conjecture that wind statistics in (x, y, z') -space might be horizontally homogeneous. Nevertheless for present purposes it was of interest – as one possible strategy for inverse dispersion – to represent each detector path, not as a straight line (e.g. at the mean height $\langle z'_{C39} \rangle = 1.43$ m or $\langle z'_{C15} \rangle = 1.65$ m) but as a spatial sequence of “point” detectors (or rather, short line-segments), each of which could be assigned a height $z'(x, y)$ at will. The latter is a means to reframe the tracer dispersion experiment in a ground-following coordinate, transforming the straight line laser light paths of (x, y, z) -space into curved light paths in (x, y, z') -space (Fig. 2.4).

This is one of three strategies tested for representation of the detector paths, and it will be referred to below as the terrain following coordinate. Specifically, each line-averaging laser light path was represented in the analysis by 20 point gas detectors, these being evenly spaced (with interval 5.8 m) between the emitter/detector and the reflector. Each of these point detectors could (optionally) be assigned its own true height $z' = z - h(x, y)$ above the local ground surface (terrain-following coordinate), or, some other choice.

1.12 Results

The first objective was to determine what would be an optimal strategy for performing the inversion $(\bar{c}_u - \bar{c}_d) \rightarrow Q_{IDM}$ given *complete* information on the spatial distribution of the source (i.e. eight equal point sources, each at known x, y, z), bearing in mind the known irregularity of the terrain (whose detailed implications for the wind field would remain unknown) and the conviction (from past experience) that it would be necessary to exclude certain observation intervals (occurring under a too extreme stratification, or during a mean wind direction too closely aligned with the long axis of the plot). Beyond that, and knowing that in the upcoming trials the sources (cattle) would not necessarily be fixed in space nor necessarily equal in strength,

it was natural to wonder whether the inversion might be more or less vulnerable depending on how the source were represented: perhaps as an area source at an estimated mean head height, or as a volumetric source (plot area \times standing head height), and so forth.

In terms of organization, we first look sensitivities to filtering criteria in regard to the micrometeorological state, treating the detector light paths as curved beams at their true height above local ground (terrain following coordinate). We then visit alternative representations of the detector beams, followed by alternative assumptions in regard to the source distribution. It may be worthwhile to remind the reader that, throughout, the inversion is based on concentrations \bar{c}_u , \bar{c}_d measured by the two lasers in the tracer experiment, even where (for the purposes of the sensitivity study) the positions of those lasers have in some cases been intentionally misrepresented. Recall too that Q_{IDM}/Q is the ratio of the calculated emission rate Q_{IDM} to the true emission rate Q , with $Q_{\text{IDM}}/Q = 1$ representing the perfect accuracy. Of course, the more rigorous or aggressive the filtering applied, the fewer the measurement intervals contributing to a determination of source strength; one can anticipate that a compromise must be reached in this regard.

1.12.1 Sensitivity to filtering criteria

The impact of each of the following filtering criteria was assessed when implemented alone (i.e. without any other filtering), and with the detector beams represented as curved light paths in (x, y, z') -space (the terrain following coordinate).

1.12.1.1 Surface roughness length

Four alternative ensembles of runs were defined, by eliminating runs for which the roughness length⁹ exceeded an upper threshold value $z_0^{\text{thres}} = (0.05, 0.1, 0.15, 0.25)$ m. Across these ensem-

⁹The apparent roughness length for each interval was diagnosed from data provided by the sonic anemometer, specifically the mean horizontal wind speed, the magnitude u_*^2 of the kinematic vertical momentum flux density, and the kinematic virtual heat flux density $\overline{w'T'_v}$. By optimization of the roughness length z_0 (treated as flexible,

bles the mean performance as defined by $\langle Q_{\text{IDM}}/Q \rangle$ varied without regularity from approximately 1.08 to 1.09, and there was (likewise) no pattern in $\sigma_{Q|Q}$. Therefore in the following analysis no data were rejected on the basis of the roughness length.

1.12.1.2 Mean wind direction

Based on the geometry of the experiment, it was evident that the point detectors would not detect a meaningful concentration difference whenever the wind blew nearly parallel to the long axis of the plot, i.e. from the north or from the south. If observations were rejected for periods of northerly or southerly winds by rejecting data for which $\bar{\beta}$ lay within sectors spanning $\pm 30^\circ$ or $\pm 20^\circ$ or $\pm 10^\circ$ about due north (or south), the mean ratio over all retained intervals improved markedly from $\langle Q_{\text{IDM}}/Q \rangle = 1.09$ (no filtering based on mean wind direction) to $\langle Q_{\text{IDM}}/Q \rangle = (1.04, 1.04, 1.04)$ respectively, while the standard deviation decreased from $\sigma_{Q|Q} = 0.33$ (with no filtering based on mean wind direction) to $\sigma_{Q|Q} = (0.12, 0.13, 0.15)$ respectively. Thus rejection cones spanning $\pm 10^\circ$ about $0/360^\circ$ and 180° suffice to filter out periods having an ambiguous wind direction.

1.12.1.3 Friction velocity and Obukhov length

Fig.2.5 summarizes the performance of inverse dispersion (as characterized by $\langle Q_{\text{IDM}}/Q \rangle$) for different combinations of u_* and $|L|$ rejection thresholds, the leftmost column corresponding to $|L| \geq 0$ (i.e. no filtering whatsoever in regard to L). If data are rejected for intervals having friction velocity below a threshold value $u_*^{\text{thres}} = (0.05, 0.1, 0.15) \text{ m s}^{-1}$ the mean performance improved slightly from $\langle Q_{\text{IDM}}/Q \rangle \approx 1.05$ (no threshold) to $\langle Q_{\text{IDM}}/Q \rangle \approx (1.04, 1.03, 1.02)$, while the standard deviation remained constant at $\sigma_{Q|Q} \approx 0.12$.

Earlier tests (Flesch et al. [2005]; Flesch et al. [2014]) have reported a little improvement in the accuracy of the inverse dispersion method when a threshold magnitude L^{thres} for the Obukhov length is imposed (i.e. runs are rejected when $|L| < L^{\text{thres}}$). In the present experiment

run by run) these data were required to conform to the Monin-Obukhov mean wind profile.

such a filter did not result in a convincing improvement in the accuracy of the inversion for Q_{IDM} , for while the bias and scatter do decrease when runs having $|L| < 8$ m are rejected, such that $\langle Q_{\text{IDM}}/Q \rangle$ falls from about 1.04 to 1.02 and $\sigma_{Q|Q}$ from around 0.16 to 0.12, the bias increases again so soon as a larger threshold magnitude is imposed. Of course it is in the nature of the averaging process that the pattern shown in Figure 2.5 may reflect idiosyncrasies of the data, i.e. the retention or rejection of a given run having Q_{IDM}/Q very different from unity can explain the irregularity of the pattern.

1.12.2 Effect of representation of detector beams

As simpler alternatives to the adoption of a curved beam height (the “terrain-following” paradigm, strategy **A**), two simpler strategies using constant laser light path height were tested:

- B.** for each beam, use the average of detector height above ground and reflector height above ground: this yields $\langle z'_{\text{C39}} \rangle = 1.43$ m and $\langle z'_{\text{C15}} \rangle = 1.65$ m
- C.** for each beam, take the average of the beam height above ground every 20 m from the south end of the paddock ($y = 10$ m) to the north end ($y = 110$ m): this yields $\langle z'_{\text{C39}} \rangle = 1.40$ m and $\langle z'_{\text{C15}} \rangle = 1.30$ m

Table 1.1 summarizes the outcomes for these three strategies. With strategy A (the terrain following coordinate) the inversion gives $\langle Q_{\text{IDM}}/Q \rangle = 1.04$ and $\sigma_{Q|Q} = 0.15$. Using strategies B and C however, the mean ratios are $\langle Q_{\text{IDM}}/Q \rangle = (1.59, 1.04)$ and the standard deviations $\sigma_{Q|Q} = (0.88, 0.17)$ respectively. We conclude that compensating for the variable (actual) height of the detector beams above ground improves accuracy, and that (by a small margin) strategy **A** (the terrain following coordinate) is best. The relative merits of strategies **A** and **C** may well hinge on particularities, and differ in other experiments.

1.12.3 Alternative representations of the source

For the results given above, the detected concentration signals were inverted with the à priori knowledge that the concentration field had been caused by eight point sources of equal strength and all the same height (0.8 m), these being irregularly distributed but at known positions. Recall too, that the actual distribution of the sources along the y -axis has no impact on the line-averaged concentrations detected by the lasers.

But supposing one did not know the source distribution: how should the source best be represented? Are some assumptions liable to be safer than others? In general, two broad options apply, i.e. representation as an area source, or as a collection of point sources. For each manner of representing the source, we tested each of the three strategies **A-C** in regard to representation of the detector beams.

1.12.3.1 Area source treatments

Since (in the sorts of applications envisaged) the animals would be fenced into a paddock, we tested the assumption of an area source with known perimeter, located on the height axis either on ground, or at an elevation of 0.8 m (same as the release height of the actual point sources, which corresponds very roughly to the effective release height of the breath of a sitting animal).

Table 1.1 gives the values of $\langle Q_{\text{IDM}}/Q \rangle$ for the area source treatments investigated. If emission is assumed to occur at the surface the outcomes of strategies A, B, and C are all poor, with $\langle Q_{\text{IDM}}/Q \rangle = 1.76, 1.84, 1.32$ and $\sigma_{Q|Q} = 1.05, 3.17, 2.42$. On the other hand if the area source is assumed to be elevated, and provided filtering based on mean wind direction was applied, strategies **A** and **C** resulted in satisfactory inversions with $\langle Q_{\text{IDM}}/Q \rangle = 1.09, 1.03$ respectively, along with tolerably small standard deviations $\sigma_{Q|Q} = 0.23, 0.21$. With strategy **B**, however, the result is poor, with $\langle Q_{\text{IDM}}/Q \rangle = 1.81$ and $\sigma_{Q|Q} = 1.70$.

1.12.3.2 Point source treatments

We studied four assumed spatial distributions of the eight point sources that (in all cases) were elevated 0.8 m above the surface; and once again, each configuration was analysed using each of the three strategies for representing detector beam height. The sources were alternatively **(a)** spaced along the centre line of the paddock, spanning its long axis; **(b)** distributed randomly over the paddock (uniform distribution along x -axis); **(c)** distributed on the east side of the paddock (inversions restricted to wind directions $5^\circ \leq \bar{\beta} \leq 175^\circ$); and **(d)** distributed on the west side of the paddock (inversions restricted to wind directions $185^\circ \leq \bar{\beta} \leq 355^\circ$).

The results of applying strategies **A**, **B**, **C** to point sources spaced along a centre line were respectively are $\langle Q_{\text{IDM}}/Q \rangle = (1.06, 1.56, 1.03)$ (Table 1.1), and rather similar outcomes are obtained by assuming randomly distributed point sources: $\langle Q_{\text{IDM}}/Q \rangle = (1.06, 1.61, 1.05)$. However if the point sources are assumed to be distributed on either extremity of the paddock the outcomes are much inferior, with $\langle Q_{\text{IDM}}/Q \rangle = (1.22, 1.56, 1.62)$ for placement farthest and $\langle Q_{\text{IDM}}/Q \rangle = (1.39, 1.78, 1.18)$ for placement nearest to the downstream detectors.

1.12.3.3 A computational tracer experiment

For all prior results, inverse dispersion was based on actual (i.e. measured) concentrations for the given experimental period, and of course these owed to the actual – physical – source positions. However it was of interest to know what might be the consequence if all animals were *assumed* to be distributed along the centre line of the paddock, whereas *in actuality* they were concentrated along one or the other side of the paddock – these being the two extreme possibilities.

Using WindTrax in its forward Lagrangian stochastic (fLS) mode we computed a synthetic mean concentration field, specifying background concentration as 0 ppm and the emission rate of each of 8 point sources, distributed either on the eastern extremity or the western extremity of the paddock, as 1 kg hr^{-1} . The line average concentrations that would be seen by the laser detectors were then inverted using WindTrax in the backward Lagrangian stochastic mode, with

the sources treated as having been distributed *along the centre line*. By that device, an estimate of the error that might be incurred from assuming a mistaken (cross-paddock) distribution of the sources (cattle) was obtained.

With the sources of the synthetic concentration field located on the east side of the paddock, strategies **B**, **C** respectively yielded outcomes $\langle Q_{\text{IDM}}/Q \rangle = (0.49, 0.51)$, while with the synthetic sources on the west side $\langle Q_{\text{IDM}}/Q \rangle = (0.69, 0.56)$. These results suggest that a bias, amounting at worst to a factor of two in the estimated emission rate, can result in the situation that one entirely lacks information as to the true distribution of sources within the confines of the paddock.

1.13 Conclusion

The tracer experiment described above was intended to map out the feasibility of applying inverse dispersion to determine methane emission rate from a small herd of cows (circa 10 animals), appropriately confined in a long narrow paddock, but without knowledge of actual animal positions (recall that by virtue of use of the line integrating detectors, only the x -coordinate or “cross-plot” position of a source can affect the inversion).

In terms of filtering criteria to weed out intervals unsuitable for inverse dispersion analysis, we found that the most important step is to eliminate periods with unsuitable mean wind direction: for the geometry of our tracer experiment, removing periods for which $\bar{\beta} = 0^\circ \pm 10^\circ$ or $180^\circ \pm 10^\circ$ is a satisfactory compromise. Further filtering, i.e. imposition of criteria on the friction velocity and Obukhov length, proved of little advantage — in agreement with the findings of Flesch et al. [2014].

If uncertainty as to ‘animal’ position is eliminated, then despite the departure of the experimental site from the ideal of flat, uniform terrain, standard MO-based inverse dispersion using WindTrax yielded a very satisfactory estimate of aggregate source strength ($\langle Q_{\text{IDM}}/Q \rangle = 1.04$, $\sigma_{Q/Q} < 0.2$), and this regardless of whether one treated the detector as a curved light path at actual beam-height-above ground, or assumed a constant path height equal to the average path

height alongside the paddock (these figures are very comparable with those observed in similar tracer experiments on truly flat terrain, rather to our surprise). Furthermore with the actual source distribution employed here, which mimicked ‘cattle’ spread out over the paddock so that their cross-plot distribution was not biased towards either side of the paddock, the accuracy of the inversion was not very sensitive to one’s spatial representation (in the inversion) of the effective source: excellent accuracy was obtained (with $\langle Q_{\text{IDM}}/Q \rangle = 1.03$ or 1.04) regardless of whether the tracer source was represented using the actual positions, using sources evenly distributed across the paddock, randomly distributed across the paddock, or by way of an elevated area source. Together these findings suggest the basic experimental design will provide a workable means for applying the inverse dispersion method to cattle, forgiving in terms of terrain undulations and free of the need to monitor animal positions.

There are however two concerns with the design. First is the sensitivity to assumed source height, for while the inversion yields good accuracy in $\langle Q_{\text{IDM}}/Q \rangle$ when the true source height is used (e.g., area source at height 0.8 m) the outcome is poor if that area source is placed on ground (this of course is a consequence of the close proximity of the downwind detector to the source). When measuring enteric emissions (from the breath) the mouth height of the cattle is unlikely to be known with accuracy, and this sensitivity to source height is undesirable. The second concern is the level of inaccuracy that could occur if cattle congregated on one side of the paddock: quantified using synthetic data created with WindTrax (using the actual wind statistics collected during the tracer release) a (maximum) bias of up to a factor of two in the estimated emission rate would occur if the cattle were to remain congregated at one side of the paddock. A further sensitivity study (not reported above) suggested this (worst case) bias would be much less serious were the laser paths to be placed some 5 m more distant from the paddock boundaries.

Acknowledgments

This research has been funded by a grant from the Agricultural Greenhouse Gases Program of Agriculture and Agrifood Canada, and by the Natural Sciences and Engineering Research Council of Canada. The authors acknowledge the assistance of Peter Carlson (Dept. Earth & Atmospheric Sciences, University of Alberta).

Table 1.1: Performance of inverse dispersion in relation to one’s assumption in regard to the source distribution, and one’s representation of the height of the detector beams. The bottom two rows give the result of inverting a synthetic concentration field, mistakenly treating the sources as being on the midline of the plot whereas (for the purpose of constructing the concentration field) they actually were on the west or east side of the plot.

Assumed source distribution	Strategy A	Strategy B	Strategy C
True point sources	1.04 (0.15)	1.59 (0.88)	1.04 (0.17)
Surface area source	1.76 (1.05)	1.84 (3.17)	1.32 (2.42)
Elevated area source	1.09 (0.23)	1.81 (1.70)	1.03 (0.21)
a) Even point source	1.06 (0.15)	1.56 (1.02)	1.03 (0.15)
b) Random point source	1.06 (0.17)	1.61 (0.97)	1.05 (0.16)
c) Point sources on east side	1.22 (0.77)	1.56 (0.48)	1.62 (0.64)
d) Point sources on west side	1.39 (1.47)	1.78 (0.58)	1.18 (0.22)
Midline (synthetic source east side)		0.49 (0.84)	0.51 (1.53)
Midline (synthetic source west side)		0.69 (0.58)	0.56 (0.60)



Figure 2.1: A view of “plot 22” looking towards the north from the southern boundary fence. The origin of the coordinate system lies at the junction of the two visible fences, just out of sight at the lower left of the photograph. The light path of the laser gas detector at lower left runs northward, parallel to the fence defining the western boundary of plot 22, to a reflector seen just below the skyline. Also visible: cup anemometers, elevated gas release points, and a sonic anemometer at the right of the photo. The distance along the western fence from the origin to the gate on the skyline is 290 m.

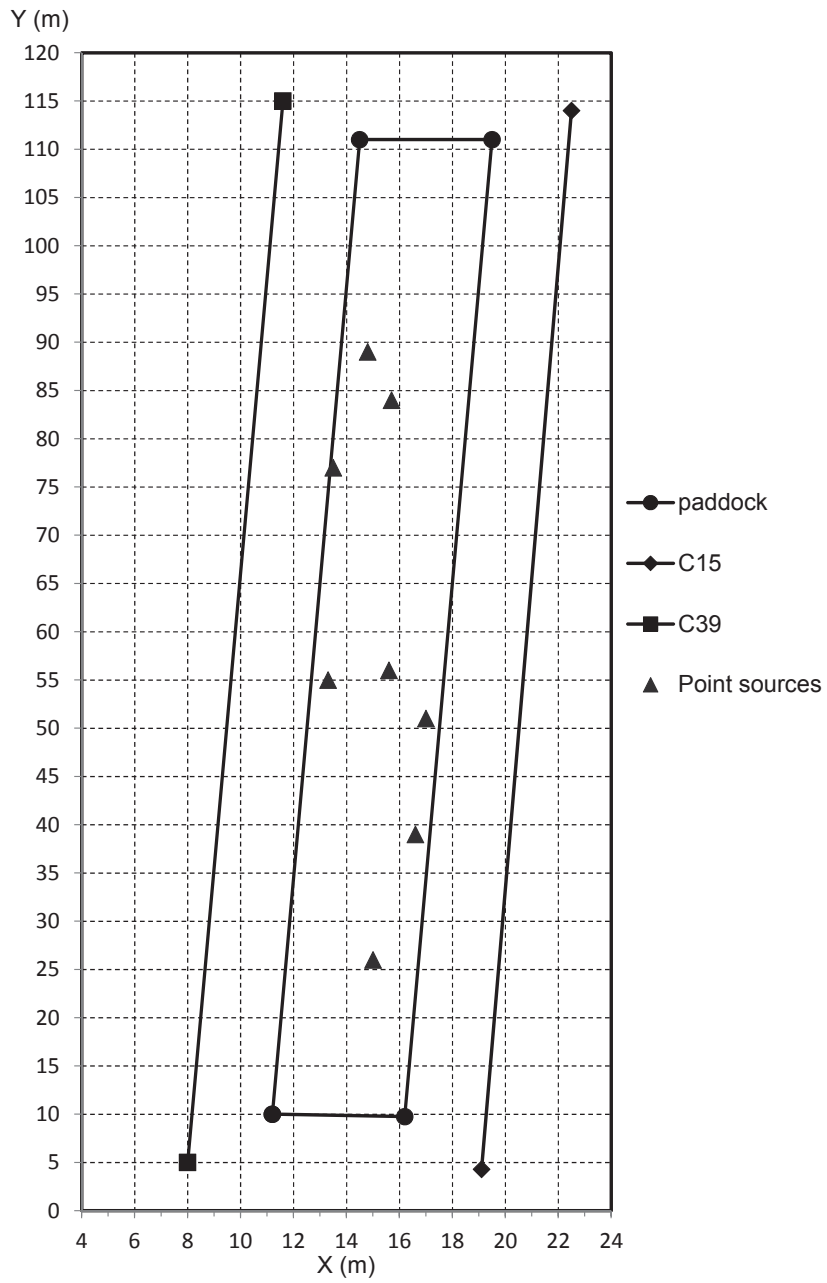


Figure 2.2: Sketch of plot 22. Light path of detector C39 spans $(x, y) = (8, 5)$ to $(11, 115)$, while light path of detector C15 spans $(19, 4)$ to $(23, 114)$.

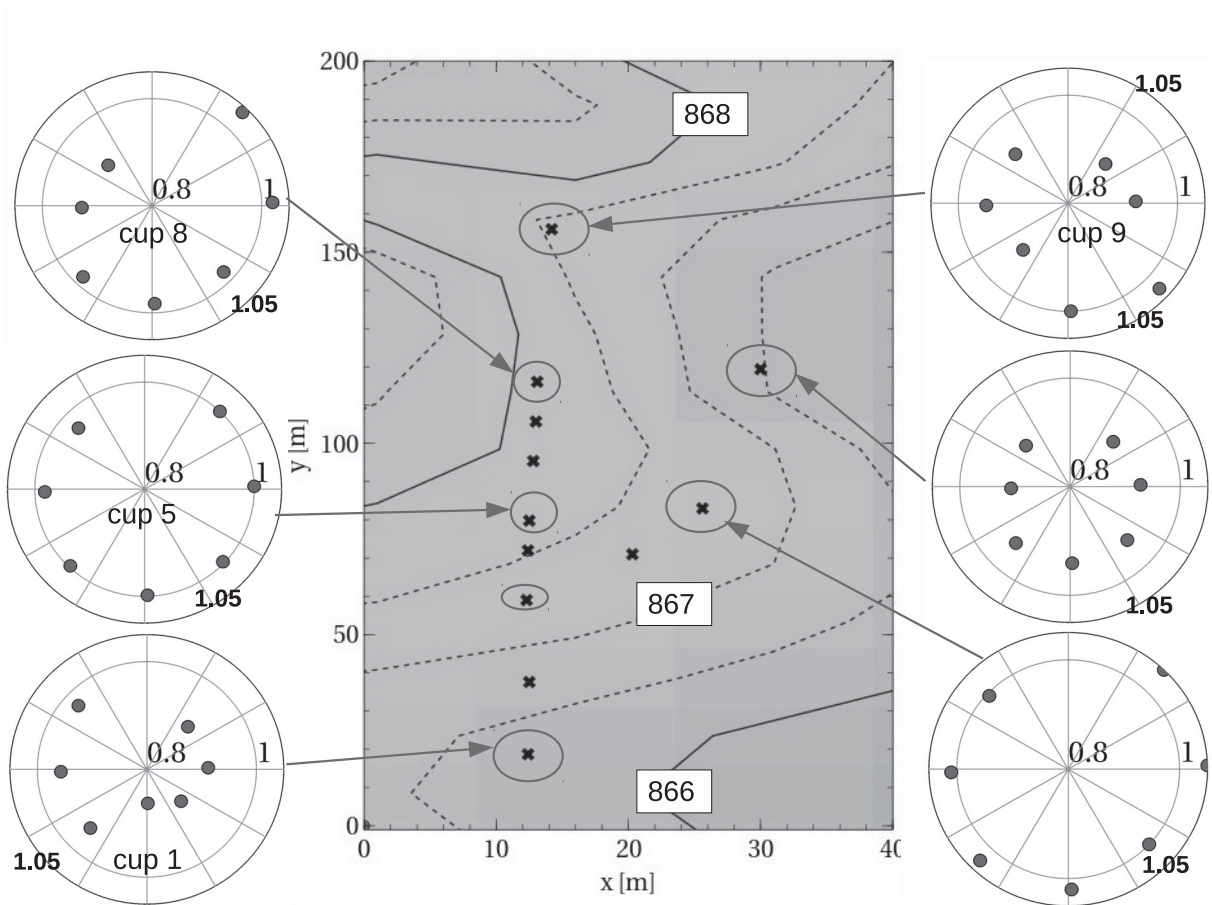


Figure 2.3: A view of the terrain (contour elevations in m), with positions of cup anemometers (crosses) and associated wind roses. Each wind rose gives the mean relative wind speed within each wind direction sector (the reference anemometer is the third from the bottom). The relative windspeed axis spans the range 0.8 – 1.05.

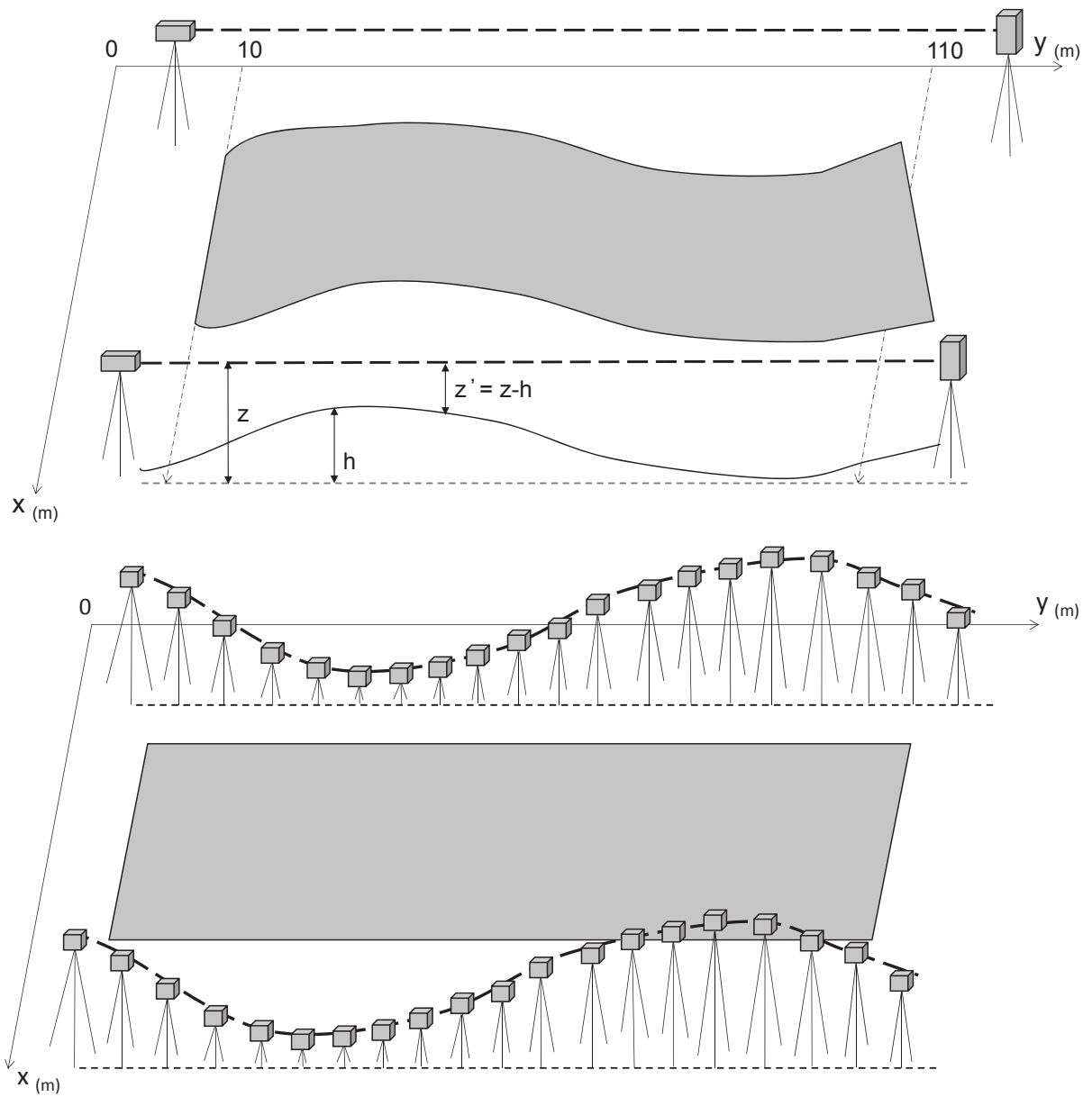


Figure 2.4: Upper panel: definition of terrain following coordinate for detector height. Lower panel: detector light paths, curved after adopting terrain following coordinate.

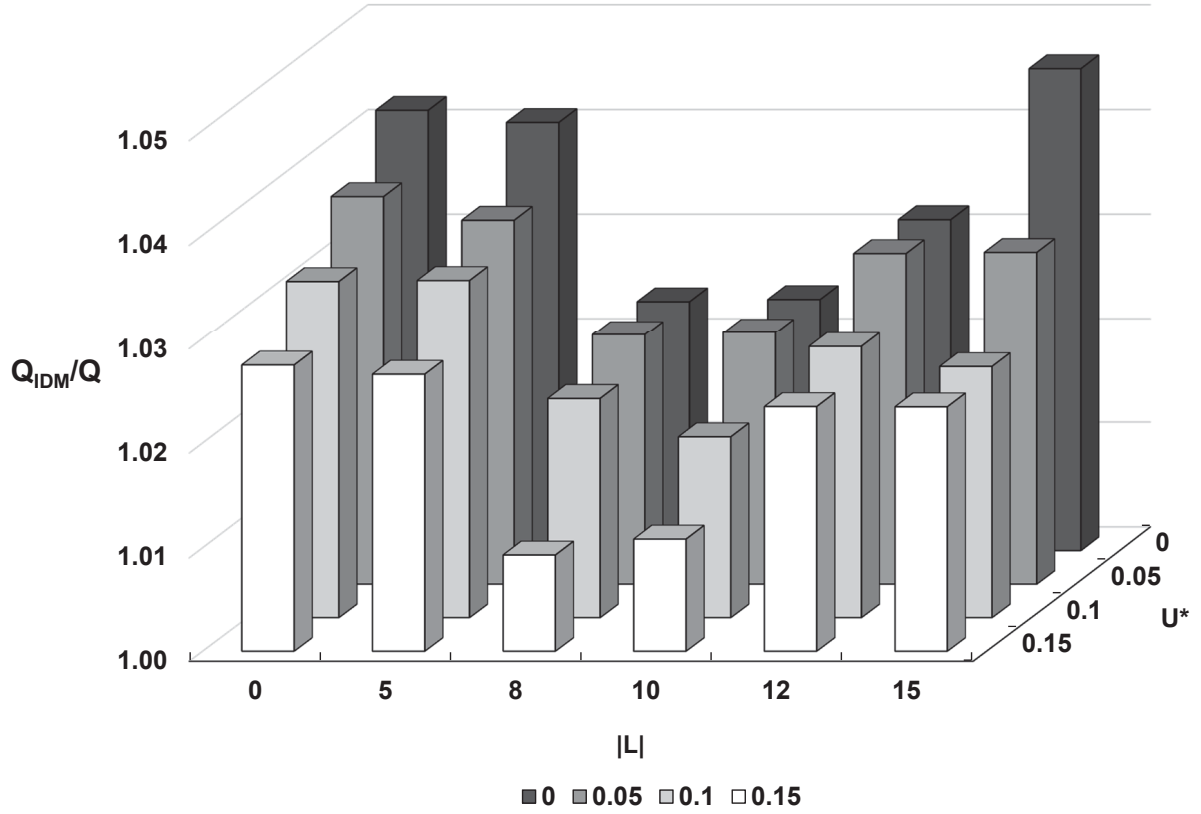


Figure 2.5: Mean performance $\langle Q_{IDM}/Q \rangle$ of the inverse dispersion method in relation to the imposition of filtering based on imposed *minimum values* for the magnitude $|L|$ [m] of the Obukhov length and for the friction velocity u_* [m s^{-1}]. The leftmost column corresponds to $|L| \geq 0$ (i.e. no filtering in regard to L), while the rear (black) row corresponds to $u_* \geq 0$ (i.e. no filtering in regard to u_*).

Chapter 3. Application: methane emissions from narrowly-penned cattle

The results conveyed in Chapter 2 suggested a promising avenue for the adaptation of the bLS approach to measure methane emission from cattle outdoors, feeding naturally, and only loosely constrained in terms of their movements. Given the propensity of animals to respond to their environment, and particularly where this is severely unnatural (as in, for instance, laboratory gas exchange chambers; or where they are forced to wear intrusive and bulky gas detection equipment), this is a salient advantage of the bLS methodology.

The present chapter will describe such a bLS experiment on animals feeding in long, narrow plots, and will compare the inferred emission rate with a calculation based on the “tier 2 protocol” of the 2006 Intergovernmental Panel on Climate Change (IPCC). As throughout this thesis, the focus is not so much the numbers in and of themselves, but on the credibility of methodologies — and particularly inverse dispersion by MO-bLS — by which they may be estimated.

It will also be of interest to demonstrate a capability of bLS not illustrated in Chapter 2, where source strength was uniform in time. Animals, whether managed or free, have their daily patterns, and the high temporal resolution of the bLS method, i.e. order 30 min, permits to resolve the diurnal course of the emission rate. It will be obvious to the reader that the methodology has generality, e.g. assuming the availability of a suitable detector, it could be (and indeed has been) used to determine the flux of ammonia volatilized from cattle urine.

3.1 Site, instruments and methodology

An experiment to determine cattle methane emissions using inverse dispersion by MO-bLS was performed during August 2013 in “plot 4” at the Lacombe Research Centre (Agriculture and Agri-Food Canada, 52.457605 N, 113.760424 W; see Figures 3.1-3.4). Plot 4, the north-west

corner post of which serves as coordinate origin, had been split by readily moved, single-wire electric fencing into five long, narrow strips, each 5 m wide and approximately 260 m in length (the long axis was oriented roughly north-south). The choice of long, narrow enclosures for the cattle was made to ensure that for almost all mean wind directions the herd methane plume would pass across the downwind detector light paths, and result in significantly different upwind and downwind concentrations (as for the tracer trials described in Chapter 2). On five days sequentially, a herd of twenty cattle was given access to graze these narrow strips, one strip after another (i.e. each morning they were moved to the adjacent strip in the succession, moving from strip 1 on the east towards strip 5 on the west; see Figure 3.4). Strip lengths were varied based on the estimated forage amount (more specifically, it was selected so that the available forage amounted to 7% of the herd body weight), and each strip had potable water and mineral to which the animals — heifers — had ad libitum access. Because (all else being equal) methane emission rate is proportional to feed intake, the animals' daily consumption was inferred from regular sampling of the pasture, a monoculture of fleet meadow brome grass (*Bromus riparius Rehm*).

As in Chapter 2, a single sonic anemometer provided the needed meteorological information. However in terms of the gas detection equipment, this trial differs from Chapter 2 in that here only a *single* line-averaging laser gas detector was used (again, a Boreal Laser Gasfinder 2). This was possible because the source/detector unit was mounted on a motorized and computer controlled tripod, so that the beam could be directed in sequence to up to four remote cube retro-reflectors (see Fig 3.3). In order that all four paths should be aligned with the long axis of the strips, the detector on its mount was positioned midway down the long axis of the strips, and between 5 m (first day of two-day sequence) or 10 m (second day) eastward of the strip occupied by the cattle. Two light paths ran (roughly) 130 m north and south to reflectors, such that signals along those two paths could be combined to give the east-side line-averaged concentration. To obtain the concentration on the *west* side of the strip, two plane mirrors (see Fig 3.3) were placed “opposite” the source/detector, i.e. at the midpoint of the long axis of the

strip, but each 10 m (first day of two day sequence) or 5 m (second day of sequence) westward of the west side of the strip. One plane mirror redirected the beam to a reflector to the south¹⁰, and the other to the north. Thus in effect there were four light paths, each parallel to the long axis of the strip, so as to be able to define an “upwind” and a “downwind” line-average concentration. We identify these four paths as lines (1,2) linking the detector to the south-east and north-east reflectors, and lines (3,4) linking the detector *via the plane mirrors* to the north-west and south-west reflectors. The short “cross-strip” pathlength of lines (3,4) was *assumed to be exposed only to background concentration*, and to ensure this was the case periods when the wind could have carried methane from one or more animals into those paths were *eliminated* from the analysis. This was done on the basis of available photographs of the herd, taken at 5 minute intervals, in conjunction with a consideration of the prevailing wind direction over the interval represented by the photograph. In short the path length of each west side beam was equated to the distance from the plane mirror to “its” retro-reflector, and runs were selected in such a way as to avoid contamination of the signal.

Another deviation from Chapter 2 is a consequence of the fact that here the sources are *mobile*: that being so, and given that one does not *know* in detail where they are, how should the beam height above local ground be weighted? If one were to transform the straight light path to a curve what is important is that the beam height above ground be correct *where the beam is intercepting a gas plume*, yet in this case those plumes, tied to the cattle, are mobile. It makes sense, then, to use a fixed beam height assigned the average value along the path, particularly since in the configuration of the tracer trials, i.e. as strategy C of Chapter 2, this approach performed well. Based on measured local beam heights every 20 meters, the four reflector heights were adjusted to give the same average laser-to-reflector path height for paths 1 and 2 (which were combined as path A) and paths 3 and 4 (combined as path B), the paths

¹⁰Note that whereas, irrespective of their exact orientation, the cube retro-reflectors at the remote ends of the light paths reflect the beam *exactly* back along the path of incidence, the plane mirrors, inducing a Snell’s law reflection, needed to be oriented with some precision.

from the emitter/detector to the plane mirrors having being discounted from the latter. The mean path heights for path A (on the east side) and B (on the west side) were respectively $\langle z'_A \rangle = 1.20$ m and $\langle z'_B \rangle = 1.59$ m (days 1,2); $\langle z'_A \rangle = 1.45$ m and $\langle z'_B \rangle = 1.71$ m (days 3,4); and $\langle z'_A \rangle = 1.59$ m and $\langle z'_B \rangle = 1.72$ m (day 5).

The cattle were herded out of their pasture strip every morning and afternoon for about an hour¹¹, during which interval the concentrations measured on paths 1–4 could be assumed to represent background. This provided a twice-daily opportunity to extract a multiplicative correction factor for each of the line-averaged concentrations, in order to compensate for the known sensitivity of the returned signals to particularities of the retro-reflectors.

3.2 Inverse dispersion analysis and results

The inverse dispersion calculation to obtain Q_{IDM} was performed using WindTrax along standard lines, with the following choices:

- cattle were treated in aggregate as an area source at height $z_{src} = 0.8$ m
- threshold values for u_* and $|L|$ were respectively 0.05 m s^{-1} and 2 m
- cones of unacceptable (rejected) mean wind directions were defined as $0^\circ \pm 10^\circ$ or $180^\circ \pm 10^\circ$ *relative to the long axis of the plot* (i.e. these are not angles relative to true north)

With the above filtering, the final dataset consists of 110 30-min emission observations taken over five successive days. The goal was to estimate the daily average emission rate (per head) of the study herd, a task that was complicated by the non-continuous observation record which resulted from data filtering, offline equipment, etc. In particular, the dataset has many more daytime than nighttime observations (daytime biased) due to occurrence of low nighttime wind

¹¹For faecal sampling and the consumption of a feed that would permit to compute each animal’s dry matter intake (DMI), using a paired n-alkane methodology; those data were not available at the time of writing this thesis.

speeds that resulted in a friction velocity lower than the filtering threshold, and the nighttime occurrence of fog and dew that obscured the laser reflectors and resulted in lost data. And because cattle emissions typically have diel variability, where emissions are higher during the day than at night (e.g., van Haarlem et al. 2008), the simple average of emission from a daytime biased dataset can give an over-estimate of daily emissions.

To avoid this problem daily average rates were calculated from an ensemble-averaged daily (24 h) emission curve. It was assumed that the five days of the study data are replicates of an “average day,” which allowed the individual observations to be grouped by time-of-day. Three hour blocks were chosen, such that eight 3-h blocks cover the 24 h day. All valid emissions estimates falling within a given 3-h block were averaged to give a representative value for that particular time window, and the average of those 8 rates provided the daily average emission rate.

Figure (3.5) shows the pattern of emissions inferred by inverse dispersion over the course of the “average day.” There is large variability in emissions over the day, with low emission values in the mid-morning, and high values in the early evening. On first sight this may seem surprising, but it is in fact quite comprehensible. Arriving on fresh pasture each morning at 09:00 having exhausted and trampled the previous day’s (parsimoniously allotted) feed, the cattle began feeding enthusiastically. Their methane emission rate picked up, peaking at $Q_{IDM} = 436 \text{ g hd}^{-1}\text{d}^{-1}$ during the interval 18:00 to 21:00. During the hours of darkness some browsing continued but the emission rate declined, due presumably to intervals of sleep and perhaps less interest in feeding, as by now only the less inviting pasture remained. Even after sunrise the emission rate remained low, at $82 \text{ g hd}^{-1}\text{d}^{-1}$ from 06:00 to 09:00, reflecting the poor state of the pasture. In short, the pattern revealed by Figure (3.5) is very plausible.

The daily average of the diel emission pattern given in Figure (3.5) is $241 \text{ g hd}^{-1}\text{d}^{-1}$. This can be compared to a value estimated by the “tier 2 protocol” of the 2006 Intergovernmental Panel on Climate Change (IPCC). As noted in Chapter (1), the latter requires as input only the proportion (Y_m , dimensionless) of gross energy in feed that is converted to methane, and

the gross energy intake of the subject cattle (GE, MJ head⁻¹ dy⁻¹). According to IPCC [2006], for grazing cattle $Y_m = 6.5\% \pm 1.0\%$. The dry matter intake (DMI) for the heifers in this experiment was estimated to be approximately 10.6 kg day⁻¹ (based on 2.5% of animal body weight per day, the midpoint of the 2 – 3% value discussed by IPCC), and this was converted to GE in energy units by assuming a default value of 18.45 MJ kg⁻¹ for the specific energy density of dry matter (IPCC 2006). On this basis, the “tier 2 protocol” of the 2006 IPCC

$$EF [\text{kg}_{\text{CH}_4} \text{ head}^{-1} \text{ yr}^{-1}] = \frac{GE \times Y_m \times 365}{55.65} \quad (25)$$

yielded an emission factor $EF = 228 \text{ g h}^{-1} \text{ d}^{-1}$. This is only some 5% smaller than that the mean daily rate derived from the inverse dispersion methodology, further emphasizing the credibility of that approach.

3.3 Conclusion

This chapter has demonstrated the application of MO-bLS to quantify cattle methane emissions under a largely natural regime of management, in that the cattle were outdoors, not encumbered by any equipment, and feeding ad libidum. The estimated daily per-head methane emissions stemming from the inverse dispersion technique — an estimate that is specific with respect to site, cattle, season, pasture and time of day — has been shown to agree quite well with the highly *unspecific* and (therefore) superficial IPCC rate; it does however bear emphasis that the IPCC calculation cited above hinges on a not yet finalized estimate of dry matter intake. In any case, the level of agreement between these emission rates estimated by inverse dispersion and by the IPCC formula, while worthy of further examination when final figures are available for feed consumption, is perhaps of less interest than the demonstration here of a credible daily cycle in emission rate. Were the inverse dispersion methodology seriously wrong, it presumably would have produced an erratic daily curve of emissions, and a mean daily rate wildly out of accord with the IPCC expectation. Closing remarks follow in the next (and final) chapter.

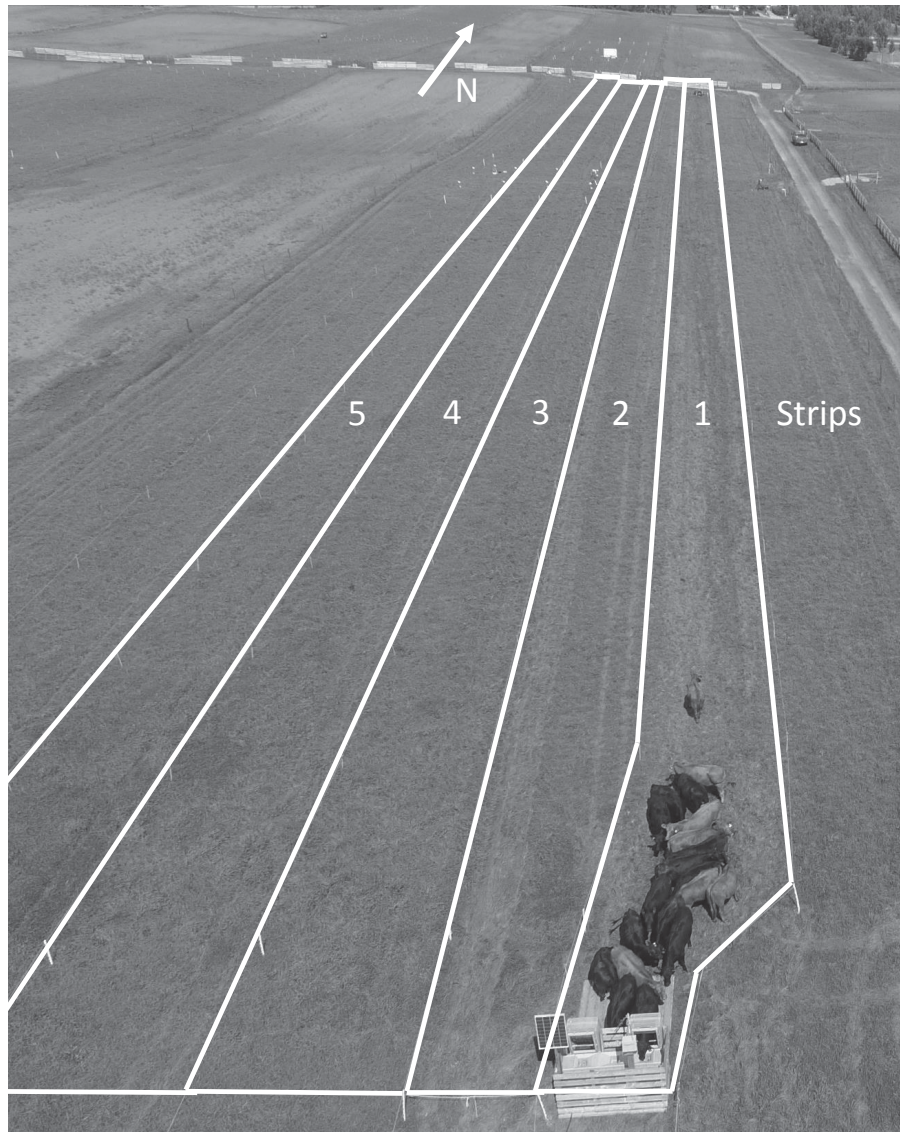


Figure 3.1: A bird’s eye view of “plot 4,” taken by a drone looking towards the north. Five fenced enclosure “strips” are identified, numbered 1 – 5 from east to west. This photograph was taken on day 1 of the experiment, at a moment when the cattle had congregated at the south end of strip 1. The laser source/detector and path re-directing plane mirrors, seen in close-up on Figure (3.4), are here barely visible towards the upper right corner of the photograph (just south of a parked vehicle).



Figure 3.2: A ground-level view of “plot 4,” taken from the south end looking towards the north. This photograph was taken on day 4, again at a moment when the cattle had congregated at the south end of the strip (i.e. strip 4). The easily-moved electric fence lines that defined the pasture strips (enclosing the cattle) can be seen. The retro-reflectors defining the nearby (south) end of the light paths are unseen “behind” the camera, such that the light paths extend beyond the extremity of the enclosure (the same being true at the north end of the strip).

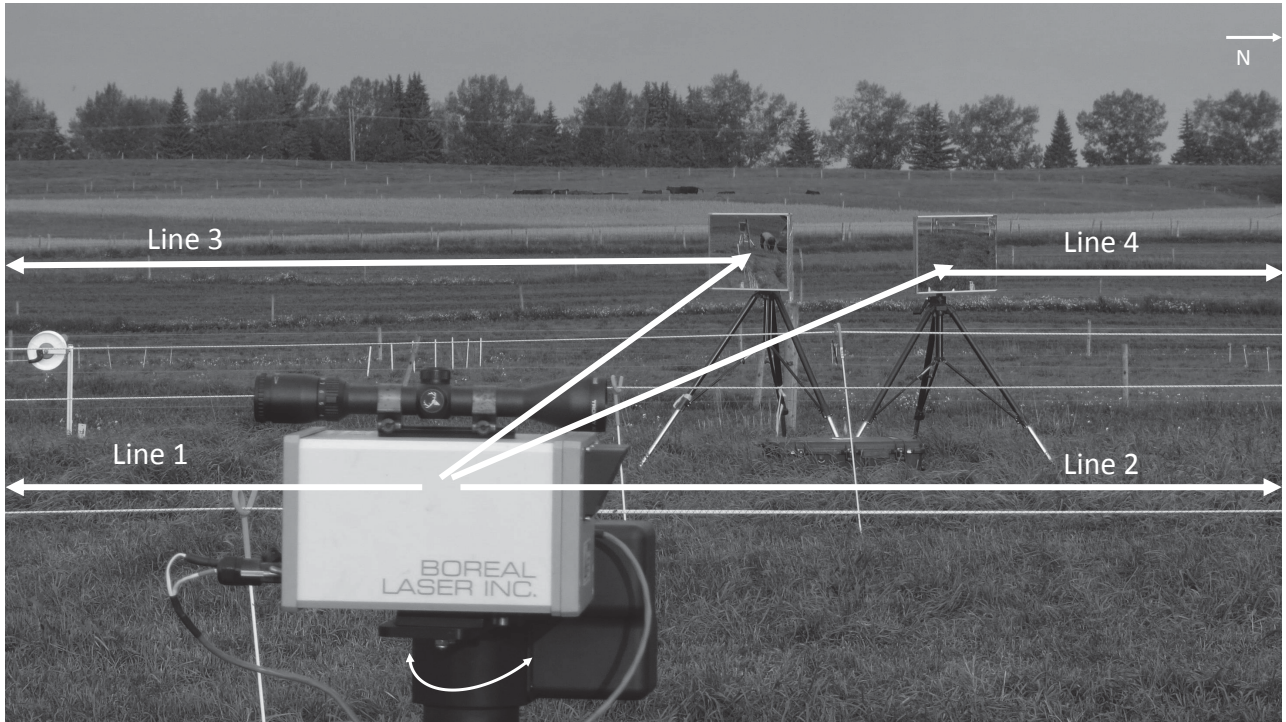


Figure 3.3: A view, looking towards the west, of the laser detector and path-deflecting plane mirrors. The source/detector is sited east of the strip enclosing the cattle, while the plane mirrors are sited on the west side of the strip. The four laser path lines from the laser source/detector are oriented towards four different distant (and unseen) retro-reflectors. Lines 1 and 2 run without redirection from the source/detector towards (respectively) the south and the north, while the plane-mirrors visible on the west side of the strip redirect lines 3 and 4 to (again, respectively) the south and the north. The photograph also conveys a sense of the gently undulating topography.

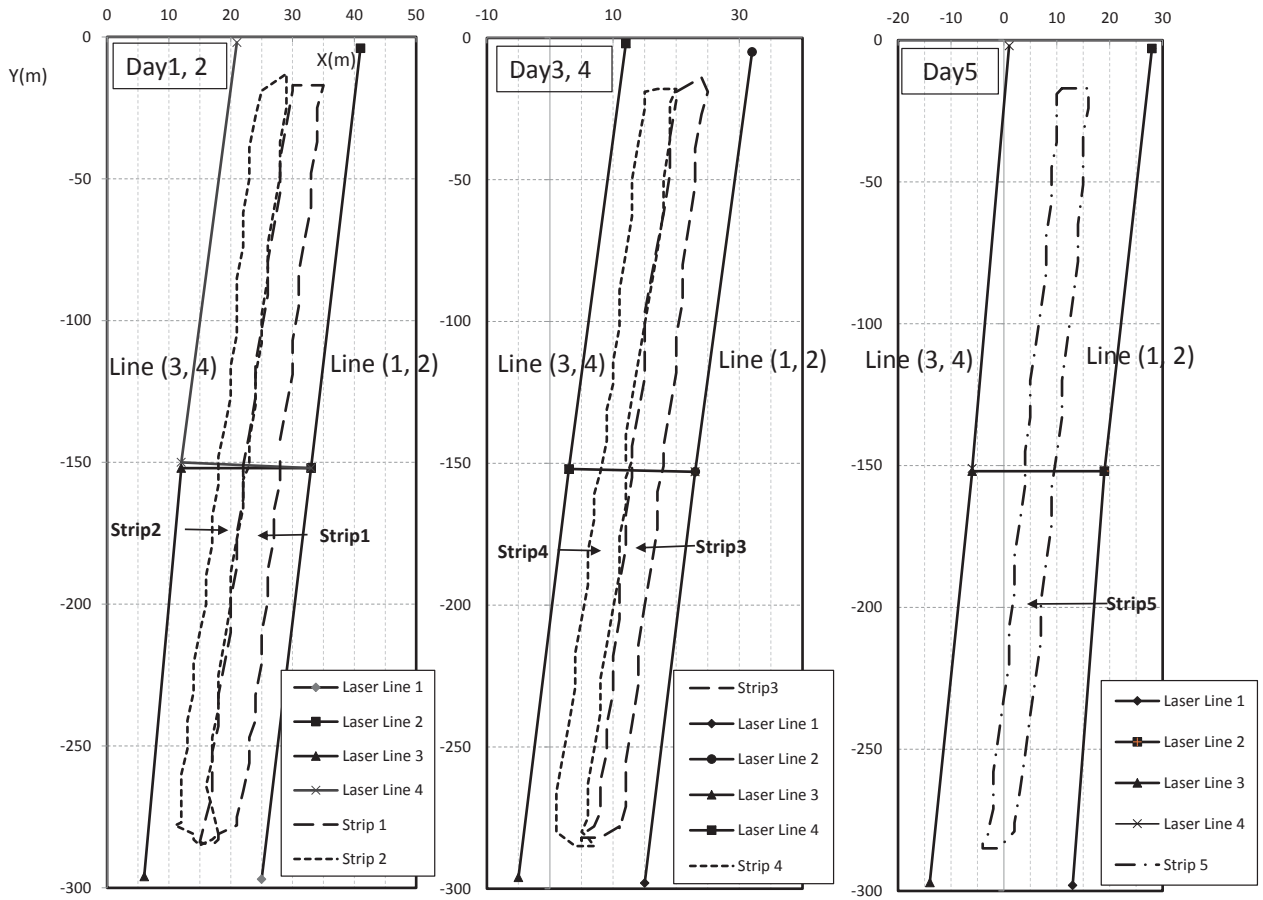


Figure 3.4: Sketch of strips 1-5 in “plot 4,” numbered from east to west. Please note the varying range of the x -axis covered by each configuration, i.e. the left-most figure, centred on strips (1&2), encloses the eastern part of plot 4; while the right-most figure, centred on strip 5, encloses the western part of plot 4. Cattle were confined within each strip for 24 hours, starting with strip 1 and being moved each morning to the adjacent strip on the west side. Each second morning the detector and light paths also were moved 10 m westward, and re-aligned.

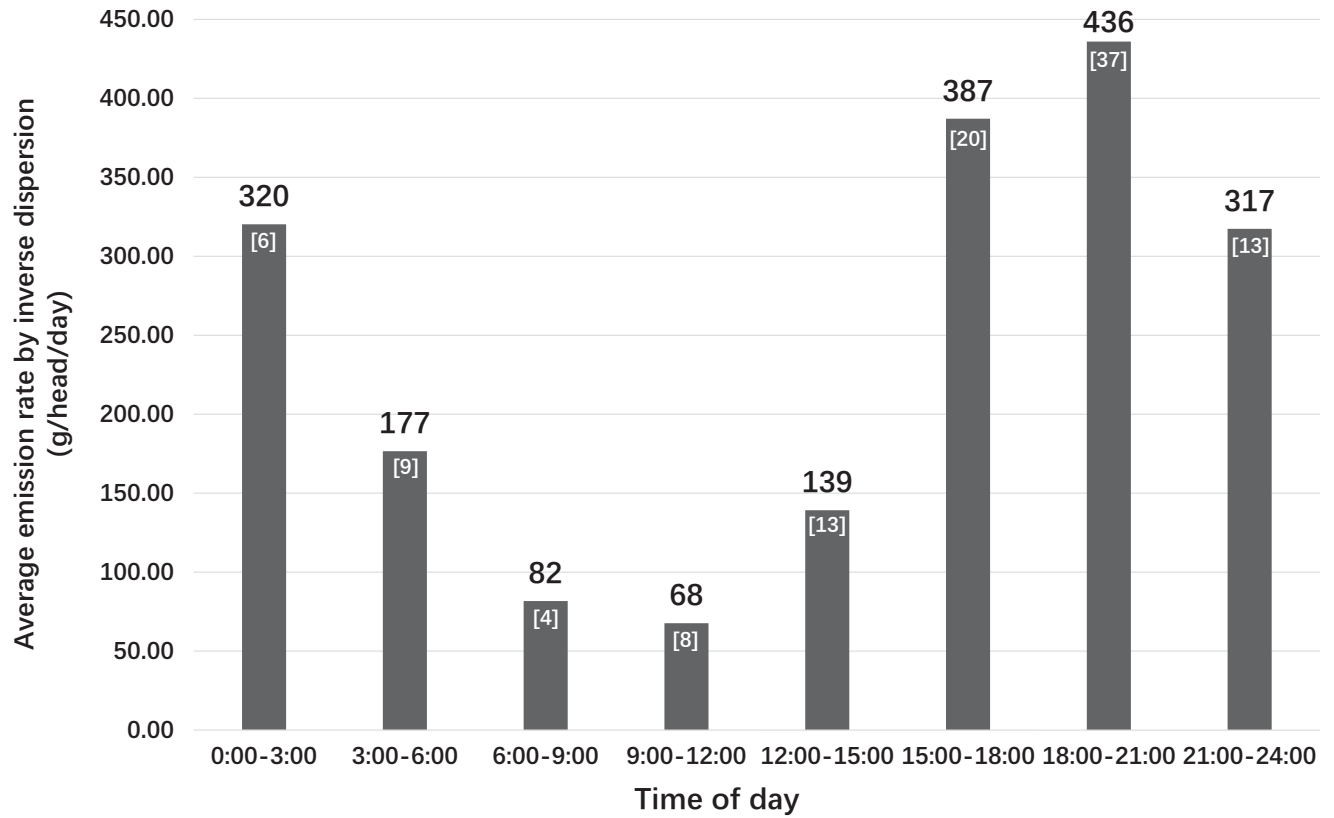


Figure 3.5: Daily cycle in the methane emission rate Q_{IDM} inferred by inverse dispersion. Three-hour averages were aggregated from the 5 days of measurements (see text), and the average across all eight bins gives a daily average methane emission rate of $241 \text{ g hd}^{-1} \text{ d}^{-1}$. The number of valid 30-min measurement intervals falling into each three-hour block is given in square brackets at the top of each bin (e.g. [4] for 6:00-9:00).

Chapter 4. Closing Remarks

Although the specific context of the work described in this thesis was the measurement of agricultural gas emissions, it should be obvious that the methodology covered has a much wider generality. It is intended that the thesis, whose subject matter might with equal validity be regarded as an element of agricultural engineering, of agrometeorology, or even of biogeochemistry, should prove accessible to interested readers from any of those fields — to which end Chapter 1 gave a quick review of those technical elements that are central to the main chapters (i.e. Chapters 2,3).

Chapter 2 has conveyed the encouraging finding that the convenient and widely used “MO-bLS” inverse dispersion method is – in the specific configuration tested, at least – robust with respect to relaxation of an underpinning assumption, namely that the wind field should be horizontally homogeneous and described strictly by Monin-Obukhov similarity theory. Chapter 2 suggests that a realistic representation of the *effective* gas detector height is pivotal, and speculates, in effect, that over modestly variable topography the atmospheric surface layer flows without perturbation, provided its properties are represented in a terrain-following coordinate¹². In fact, the wind speed measurements proved directly that this was not true of the experimental site; nevertheless, adopting the terrain following coordinate for the representation of detector height resulted in an improved, and very acceptable estimate of source strength. The extent to which this finding may generalize remains an important question. It is not apparent, however, what would be a systematic way to establish practical limits (as to acceptable terrain complications) other than by laborious trial and error along the lines described in Chapter 2.

Chapter 3 gave a very brief view of the implementation of MO-bLS in a configuration useful in the context of GHG emissions from freely ranging cattle, and the daily cycle of the inferred methane emission rate proved very plausible. Per-head daily total methane emissions inferred

¹²To some readers this may seem a daring proposition; to others, perhaps it is obvious. It is clear, of course, that as the terrain amplitude is relaxed the disturbance it causes must do likewise.

by MO-bLS were comparable with the flat rate given by the IPCC protocol, though it is stressed that the latter was based on only a preliminary estimate of one of its needed inputs (daily dry matter intake).

In closing, the MO-bLS technique as described in this thesis has been shown to have a greater flexibility of application than the principles underlying it might suggest, and it can hardly be doubted that inverse dispersion as outlined here has a useful role to play in the assessment of ground-air exchange fluxes.

References

- Australian Government, 2013: Australian National Greenhouse Accounts National Inventory Report 2011.
- Denmead OT, 1995: Novel Meteorological Methods for Measuring Trace Gas Fluxes. *Phil. Trans. R. Soc. Lond. A* **351**: 383–396.
- Environment Canada, 2013: Pollutant Inventories and Reporting Division National Inventory Report 1990/2011: Greenhouse Gas Sources and Sinks in Canada.
- Finnigan JJ, 1999: A comment on the paper by Lee (1998): “On micrometeorological observations of surface-air exchange over tall vegetation”. *Agric. Forest Meteorol.* **97**: 55–64.
- Finnigan JJ, Clement R, Malhi Y, Leuning R, Cleugh HA, 2003: A re-evaluation of long-term flux measurement techniques part I: Averaging and coordinate rotation. *Boundary-Layer Meteorol.* **107**: 1–48.
- Finnigan JJ, 2008: An introduction to flux measurements in difficult conditions. *Ecol. Appl.* **18**: 1340–1350.
- Flesch TK, Wilson JD, Yee E, 1995: Backward-Time Lagrangian Stochastic Dispersion Models, and their Application to Estimate Gaseous Emissions. *J. Appl. Meteorol.* **34**: 1320–1332.

- Hu X, Wang J, 2010: Estimation of livestock greenhouse gases discharge in China. *Transactions of the CSAE* **26**: 247-252.
- Lassey KR, 2008: Livestock methane emission and its perspective in the global methane cycle. *Aust. J. Exp. Agric.* **48**:114–118.
- McGinn SM, Beauchemin KA, Flesch TK, Coates T, 2009: Dispersion Model Performance to Estimate Methane Loss from Cattle. *J. Environ. Qual.* **38**:1796–1802
- Moss AR, Jouany J-P, Newbold J, 2000: Methane production by ruminants: Its contribution to global warming. *Ann Zootech* **49**:231–253.
- Thomson DJ, 1987: Criteria for the selection of stochastic models of particle trajectories in turbulent flows. *J. Fluid Mech.* **180**: 529–556.
- Thomson DJ, Wilson JD, 2013: History of the Lagrangian stochastic model for turbulent dispersion. *Lagrangian Models of the Atmosphere*, American Geophysical Union, Geophysical Monograph 200, 347 pp.
- U.S. Environmental Protection Agency, 2012: Inventory of U.S. Greenhouse Gas Emissions and Sinks: 1990–2010.
- Webb EK, Pearman GI, Leuning R, 1980: Correction of Flux Measurements for Density Effects Due to Heat and Water Vapour Transfer. *Quart. J. Roy. Meteorol. Soc.* **106**: 85–100.
- Wilson, JD, Thurtell GW, Kidd GE, Beauchamp EG, 1982: Estimation of the rate of gaseous mass transfer from a surface source plot to the atmosphere. *Atmos. Environ.* **16**: 1861–1868.
- Wilson J, Sawford B, 1996: Review of Lagrangian stochastic models for trajectories in the turbulent atmosphere. *Boundary-Layer Meteorol.* **78**, 191–210.
- Wilson JD, Flesch TK, Harper LA, 2001: Micro-meteorological Methods for Estimating Surface Exchange with a Disturbed Windflow. *Agric. For. Meteorol.* **107**: 207–225.

- Flesch TK, Wilson JD, Yee E, 1995: Backward-time Lagrangian stochastic dispersion models and their application to estimate gaseous emissions. *J. Appl. Meteorol.* **34**: 1320–1332.
- Flesch TK, Wilson JD, Harper LA, Crenna BP, Sharpe RR, 2004: Deducing ground-air emissions from observed trace gas concentrations: a field trial. *J. Appl. Meteorol.* **43**: 487–502.
- Flesch TK, Wilson JD, Harper LA, Crenna BP, 2005: Estimating gas emissions from a farm with an inverse-dispersion technique. *Atmospheric Environment* **39**: 4863 - 4874
- Flesch TK, Verg Xavier PC, Desjardins RL, Worth D, 2013: Methane emissions from a swine manure tank in western Canada. *Canadian J. of Animal Sci.* **93**: 159–169.
- Flesch TK, McGinn SM, Chen D, Wilson JD, Desjardins RL, 2014: Data filtering for inverse dispersion emission calculations *Agricultural and Forest Meteorology* **198–199**: 1–6.
- Harper LA, Flesch TK, Wilson JD, 2010: Ammonia emissions from broiler production in the San Joaquin Valley. *Poultry Science*, **89**: 1802–1814.
- Laubach J, Kelliher FM, Knight TW, Clark H, Molano G, Cavanagh A, 2008: Methane emissions from beef cattle a comparison of paddock and animal-scale measurements. *Australian Journal of Experimental Agriculture* **48**: 132137.
- McGinn, SM, Turner D, Tomkins N, Charmley E, Bishop-Hurley G, Chen D, 2011: Methane emissions from grazing cattle using point-source dispersion. *J. Environ.Qual.* **40**: 22–27.
- Sanz A, Misselbrook T, Sanz MJ, Vallejo A, 2010: Use of an inverse dispersion technique for estimating ammonia emission from surface-applied slurry. *Atmospheric Environment*, **44**: 999–1002
- Todd RW, Cole NA, Rhoades MB, Parker DB, Casey KD, 2011: Daily, Monthly, Seasonal, and Annual Ammonia Emissions from Southern High Plains Cattle Feedyards. *J. Environ. Qual.* **40**: 1–6.

- Thomson DJ, 1987: Criteria for the selection of stochastic models of particle trajectories in turbulent flows. *J. Fluid Mech.* **180**: 529–556.
- Thomson DJ, Wilson JD, 2013: History of the Lagrangian stochastic model for turbulent dispersion. *Lagrangian Models of the Atmosphere*, American Geophysical Union, Geophysical Monograph 200, 347 pp.
- Wilson JD, Flesch TK, Bourdin P, 2010: Ground-to-air gas emission rate inferred from measured concentration rise within a disturbed atmospheric surface layer. *J. Appl. Meteorol. Climatol.* **49**: 1818–1830.
- Wilson JD, Flesch TK, Crenna BP, 2012: Estimating surface-air gas fluxes by inverse dispersion using a backward Lagrangian stochastic trajectory model. *Lagrangian Models of the Atmosphere*, 149–161, American Geophysical Union, Geophysical Monograph 200 (349pp).
- Intergovernmental Panel on Climate Change, 2006: Chapter 10: Emissions from livestock and manure management, 2006 IPCC Guidelines for National Greenhouse Gas Inventories.
- van Harleem RP, Desjardins RL, Gao Z, Flesch TK, Li X, 2008: Methane and ammonia emissions from a beef feedlot in western Canada. *Can. J. Animal Sci.*, **88**: 641–649.